The Graphical Design Space for Primary Drying: Sources of Variability in the Dried Product Layer and Resistance and Impact on Cycle Design

– Edited Webinar Transcript 8/24/2023

Presented by Jayasree Srinivasan, Ph.D. – Research Scientist II, Baxter International, Inc.

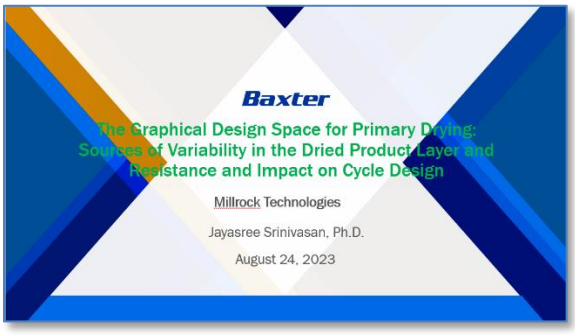

Good morning, good afternoon, everyone. My name is Jayasree Srinivasan. Please call me Jay. I'm a research scientist at Baxter BioPharma Solutions in Bloomington, Indiana. I've been with Baxter for almost eight years now, primarily focusing on formulation and lyophilization process development.

We conduct a lot of research studies. We are primarily a CMDO, but we also conduct research studies to enable publications in the betterment of the field in general. One such study that I recently conducted was on the graphical design space for primary drying. Most of you know that we develop what's called a graphical design space to optimize the primary drying conditions during lyophilization.

What are the sources of variability associated with the type product layer and the product resistance within the design space, and how does that impact the cycle design is the focus of my presentation today. So just to give you an outline of what this discussion is going to be. We will talk briefly about QbD, which is quality by design, why that is important and why it's relevant to our industry. And then we will go on to talk about the elements of a graphical design space. And then we will focus on the product resistance, which is Rp.

So, this investigation started with an assumption that the Rp is primarily constant within the design space of a given formulation. So what did we find out looking into that specific aspect of product resistance? And then we look at the formulations that we used for this study. We will analyze the data a little bit and with the conclusions, hopefully we'll have a couple of takeaways from the study and possible studies to answer some more questions.

What is quality by design? It is a multidimensional space, and more and more, the pharmaceutical industry is adapting to this quality by design wherein you develop this based on sound scientific knowledge rather than empirical or based on trial and error experiments.

As I said, these are scientifically designed based on a few performance criteria. It could be based on prior knowledge that is already existing in the literature.

And then you would develop experiments that are not redundant but based purely on a thorough understanding of a given formulation.

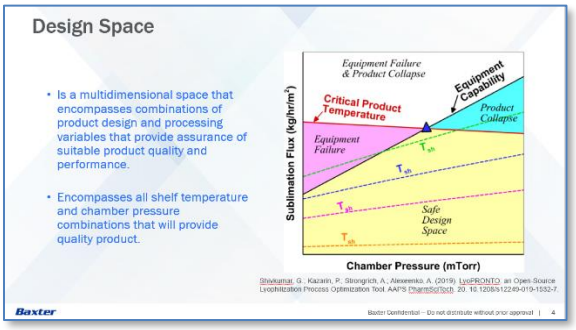

This is just a representative design space here. What it is, is a multidimensional space where you have more than two variables associated with this design space. This is primarily for the primary drying optimization with respect to lyophilization. This would be a graph of the sublimation rate on the Y axis, versus the chamber pressure on the X axis.

It encompasses a series of process conditions within this yellow region, which is called the safe zone. But then there are two boundaries that are associated with this design space. One is this red line that is your equipment capability line. That would be unique to the equipment that you are working with. On the other line here, the black line is your collapsed temperature, so which will be specific to your formulation.

This design space method is purely based on what the collapsed temperature is for your given product, what the equipment quality capability is for your lyophilizer, and also some of the parameters that are involved in developing it.

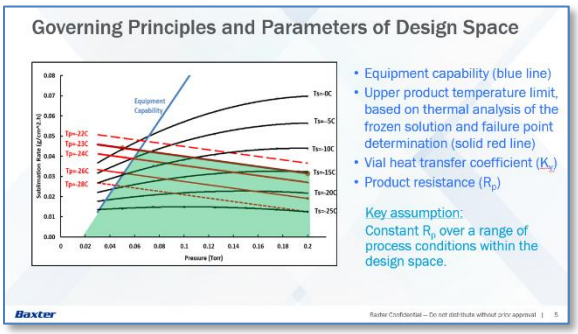

If you look at the design space with respect to how we generate it using an Excel based lyo-calculator that Professor Pecal and Steve Nail established several decades ago. So, like I said, it's a graph of sublimation rates versus chamber pressures. And this green space here is your design space.

How do we construct this design space? You know your product temperature, the collapsed temperature of your product, which is the solid red line, and you also know the capability limits of your equipment, of your dryer, which is this blue line. So, within that, using the macro of the Excel spreadsheet, the Lyo-calculator, you would input certain parameters such as the Kb, the vial heat transfer coefficient, the Rp, which is your product resistance that is unique, your product, to your formulation. And also, the other input parameters would be your shelf temperatures and other product temperatures. These are basically you're leveraging that calculator to calculate the sublimation rates at various shelf temperatures and product temperatures.

Using that, you would come up with this green zone that is well inside your capability limit and the product temperature limit. So, the assumption is that, as long as you stay inside this green space, using any combinations of shelf temperature or chamber pressure, you should be able to obtain an acceptable product. And the assumption is that the Rp, the product resistance, will be stable, constant within this green space, the safe zone.

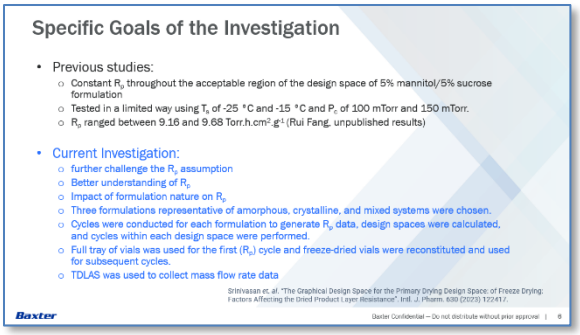

That is where this investigation started. An intern, Ray Fang, some of you may have been familiar with her, or worked with her in the past. When she interned at Baxter more than seven, eight years ago, she did a limited study, due to time constraints, on a formulation containing 5% mannitol and 5% sucrose. And then she evaluated a couple of shelf temperatures minus 25 C and minus 15 C for that particular formulation, at a couple of shelf chamber pressures.

And what she observed was somewhat similar product resistance for each of the process conditions. But then again, like I said, that was very limited data, so we wanted to probe that further. So that was the goal of this study for a better understanding of Rp. And then what are the factors that are affecting Rp? Does the Rp stay the same within the green space or does it vary? And how does it vary depending on the process conditions?

We chose three formulations, one that was representative of an amorphous system, another one for a crystalline system. And the third system was a mixed system containing both an amorphous excipient as well as a crystalline excipient. And then cycles were conducted to obtain Rp data, to generate the Rp values for these three formulations.

And from there on, we built a design space for each formulation. And then within the design space we conducted a series of cycles using various combinations of shelf temperatures and chamber pressures. We used Tunable Diode Laser Absorptions Spectroscopy to collect the mass flow rate.

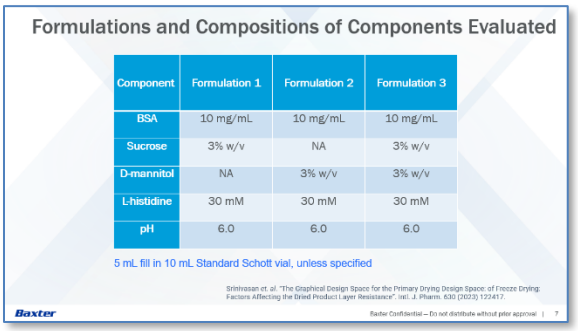

In terms of the three formulations, formulation one, like I said, was amorphous in nature, and we use BSA as the model protein at a constellation of 10 mg per Ml. So, for formulation one, we used sucrose at 3% weight to volume. It did not contain mannitol, because we wanted to keep it completely amorphous. It did contain histidine as the buffer at a pH of 6.0.

Formulation two was the crystalline system. That did not contain any sucrose, whereas it contained mannitol at 3% weight to volume.

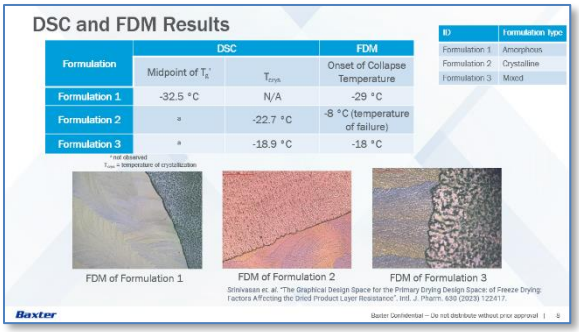

The mixed system, formulation three, contained both sucrose and mannitol. The fill volume was five Ml in a standard 10 Ml short vial, except when we used TopLyo vial, which I will specify later. In most cases we use the standard short vial.

The first step that you would conduct, as part of the development group here at BPS, we would conduct low temperature thermal analysis, just to get an idea as to what the failure point is, what the collapsed temperature is for the particular formulation. So, for that, we leverage DSC and freestyle microscopy.

Using these two studies, we found out that for formulation one, which is your sucrose formulations, I have a little table here just so I don't have to repeat it. For formulation one, the collapsed temperature was about where you would expect for a sucrose formulation, which was minus 32.5 degrees C.

And for formulation two, the crystallization temperature, because it contained mannitol, was minus 22.7 degrees C. And failure temperature, the eutectic melt, was observed at minus eight C.

And then formulation three being a mixed system, we observed a collapse at minus 18 C, and the crystallization temperature was a little warmer than it was for the mannitol formulation. These are some images during collapse or failure of the three formulations.

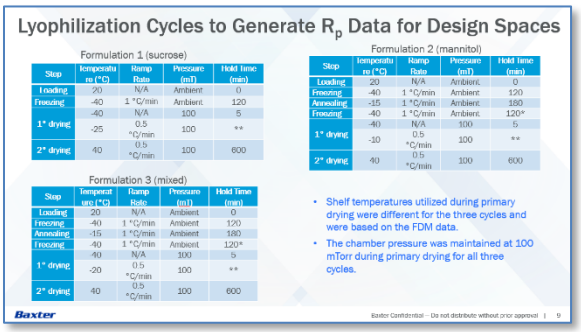

And then the next step was to go on to doing a full lyo cycle for the three formulations with an intention to generate the Rp values, and construct a design space for each of the three formulations. So the lyo cycles pretty much looked similar for the freezing step, which was down to minus 40 C, and we would hold it for a couple of hours. And the secondary drying step was also identical, with that performing at 40 degrees C, at a chamber pressure of a hundred millitorr for 10 hours.

What varied was the primary drying conditions, the parameters for formulation one, the shelf temperature was minus 25 C. And then for formulation two, in addition to the freezing step, we also had an annealing step just to encourage mannitol to crystallize completely, which was performed at minus 15 C. But primary drying was conducted at minus 10 C. For the mix system primary drying was performed at minus 20 C.

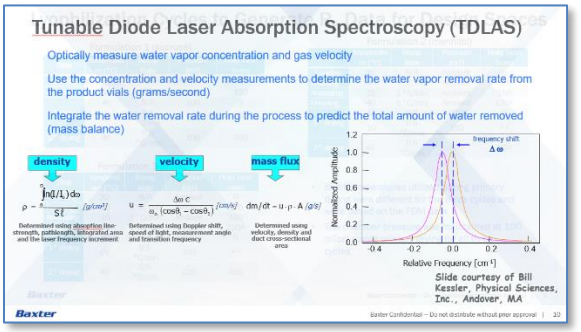

Just to give you a little bit background on the *TDLAS, if you have not used it already. What it does is, it optically measures the water vapor concentration. It is usually located in the duct area between the dryer chamber and the condenser. And then the TDLAS, it has two lasers that are positioned vertically intersecting each other. It measures the water vapor concentration and the gas velocity in the duct region, in the spool piece region. And using that information, it determines a water vapor concentration, the removal rate, which is your sublimation rate. And then it also interpolates it to determine the total amount of water lost during sublimation, and also during secondary drying. So I'm not going to go over the mathematics behind how the TDLAS works.

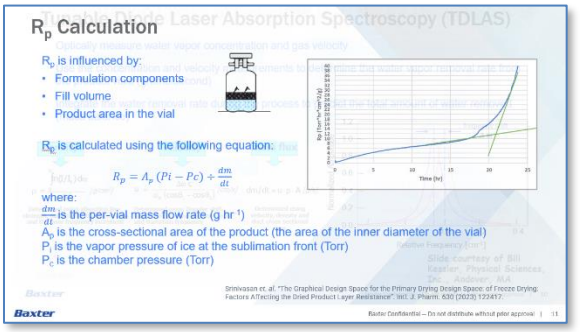

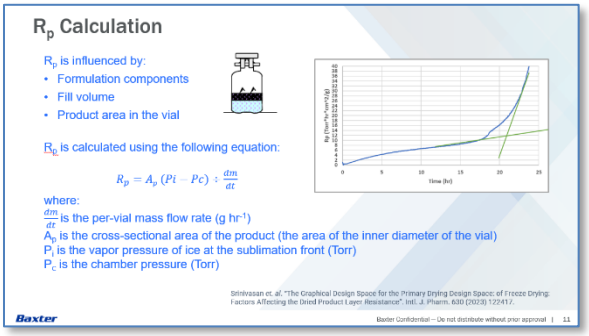

For the Rp calculation, as you can envision, Rp is influenced by the components present in your formulation, because it's different based on if your formulation is amorphous or crystalline.

It also depends on the fill volume, as you can imagine. And then the product area of the wire. So if you can visualize having a final fill in a wider vial versus a narrower vial, you can imagine the Rp is going to be much higher for the narrower vial than for the wider vial.

These are the factors that influence the Rp. And this is the principle, the mathematical principle that governs Rp, which is that Rp is inversely proportional to the mass flow rate, as you can imagine. And it directly is proportional to the area of the product inside the vial, which is the vial inner area, the diameter, and also the difference in the vapor pressure of ice at the sublimation front, which is Pi, and also the chamber pressure, which is Pc.

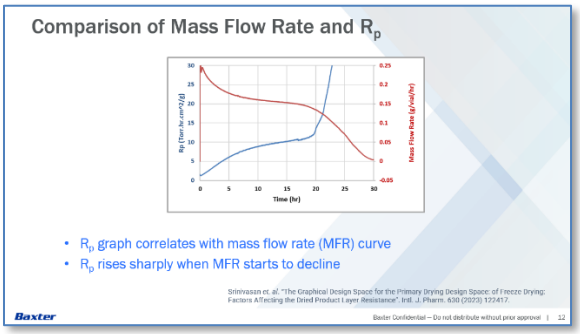

This is just a comparison of the mass flow rate that we obtained using the TDLAS, which is the red line here, and the blue line, which is the Rp data that we calculate using your product temperature and also the equation that I showed previously. You can see how well the two data correlate and compare.

If you look at the Rp lines, the Rp increases, this is just a representative curve for this particular formulation. Rp increases slowly, and at about 20 hours or so it rises steeply. So that presumably is the end of primary drying. And then if you look at the mass flow rate, it's steadily decreasing, but around the region where the Rp increases steeply, that is when the mass flow rate also decreases sharply. So that shows you that the TDLAS data that we typically use for our calculations is relatable and correlates well with the thermal couple data that you typically use to generate the Rp data.

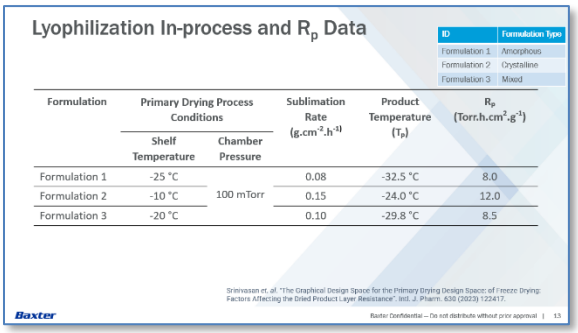

Just to summarize the product performance, all three formulations with respect to the sublimation rates, and the product temperatures, and the Rp, you can see that for formulation one, the process conditions are here. I'm not going to repeat it. The sublimation rate was at about 0.08 during the steady state sublimation step. And then the product temperature was also minus 32.5 again during the steady state sublimation. And the Rp was calculated to be about eight Rp unit.

And for formulation two, just to remind you, which is the crystalline formulation, the sublimation rate was much higher, almost a twofold increase in the sublimation rate for this formulation. And the product temperature as they would expect, was much higher because it contained mannitol in it was

minus 24 C. But then, when we calculated the Rp, the Rp was much higher for the mannitol formulation than for the amorphous formulation. So how did formulation three, the mixed system behave? The sublimation rate was somewhat similar to the amorphous formulation, formulation one, with the product temperature in between the two systems, the amorphous and the crystalline systems. And the Rp was closer to the sucrose formulation.

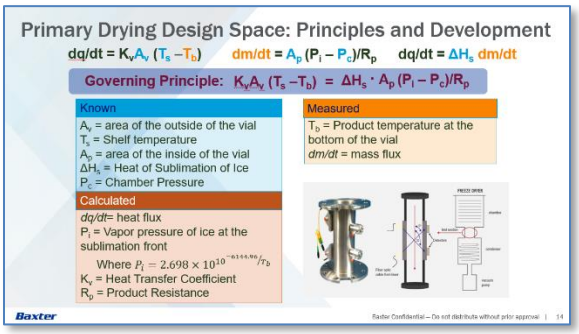

So, what is the next step then? So with that data, the Rp data, you know your vial Kv and your collapsed temperatures. The next step would be to construct the primary drying design space for the three formulations. So again, the governing principle is given here. So, what we know, these are the input parameters. Before you start your lyo run, or your Av, that's the vial area, the shelf temperature that you're going utilize for primary drying. Then the cake area, which is the vial inner diameter and the vial inner area, the heat of sublimation, which is a constant and the chamber pressure that you're going utilize for your cycle.

These are all known parameters. What you would measure using the TDLAS would be your dm or dt, which is the mass flux. And what you would also measure would be your product temperature because you would be using product thermal couples.

So what you would calculate using these equations using the first principles of heat and mass transfer would be your dq over dt here. That's your heat flux. And also the vapor pressure of ice at the sublimation front, which is the Pi. So Kv, presumably, was already obtained from a previous cycle and also Rp from a different cycle.

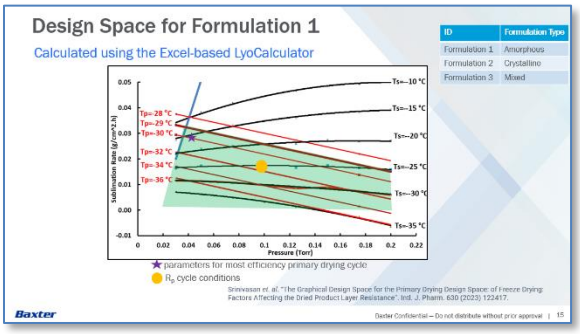

This was the design space we obtained for the sucrose formulation, formulation one, wherein the yellow circle here, the orange circle I should say, was where the cycle was conducted using a short compression of minus 25 C and a hundred millitorr chamber pressure. But then what the design space tells us is, that you can run that particular cycle more aggressively than we did here, in the sense that I could have run my cycle at minus 15 C and a chamber pressure of minus 40 or 50 millitorr.

This is how the design space is going to help you during your process development. So, imagine running your cycle at minus 15 C shelf temperature, versus minus 25 C. So, you're going to tremendously improve your cycle duration. You're going to cut down on the cycle time, the primary drying time if you were to run your cycle here versus here.

With that knowledge, the next step was to actually evaluate various combinations of shelf temperatures and chamber pressures within this green zone and see how the Rp values compare for each cycle.

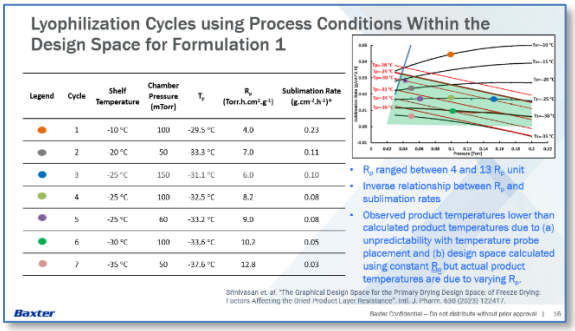

We chose a series of conditions here represented by different colored circles. And then one circle about the design space, about the green zone, I'll tell you why I evaluated that particular condition later. And then we connected a series of cycles about seven of them, and then evaluated the process parameters and also calculated the Rps and compared them.

If you were to neglect this first cycle, which was outside of the design space, if you compare the Rp data you started, the lowest was about seven and the highest was about 13. So, you see a twofold increase in Rp based on the process conditions. So the most aggressive cycle was minus 20 C, 15 millitorr, for which the Rp was the lowest. And then the most conservative cycle was at minus 35 C and 15 millitorr, wherein the Rp was about 13.

This was the general observation for all three formulations in the sense that there was an inverse relationship between the Rp and the sublimation rate. So I forgot to mention the sublimation rate. The sublimation rate was highest for the most aggressive cycle, which you would expect. And also, the lowest for the most conservative cycle.

So, there is an inverse correlation between Rp and the sublimation rate. And also, the other thing that I wanted to point out is that for example, for this particular cycle where the product temperature observed using the thermocouple was minus 33.3. Whereas if you look at the calculated product temperature over here, this particular cycle, it should have been about minus 31 or so.

The reason why we see this discrepancy, probably, was because of the placement of thermal couples. There are a lot of uncertainties associated with thermal couples. With respect to the placement, how sublimation processes, how the ice is concentrated at the center of the vial. And that makes the thermocouple move around a little bit.

And also, because the design space was calculated using a constant Rp, I told you we ran one cycle to generate the Rp data. So, it was based on that particular Rp, a constant Rp, whereas here it was calculated, but the actual product temperature was due to varying Rp because as the cycle progresses, the Rp changes. So that is why you see some differences in the actual and the calculated product temperatures.

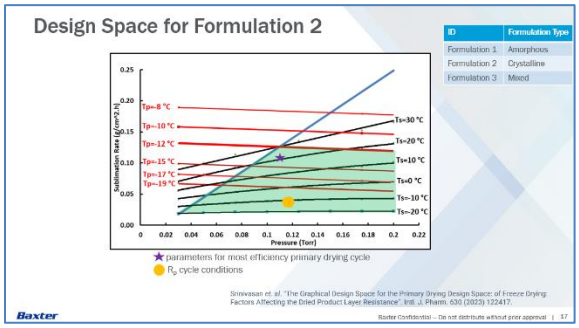

Moving on to formulation two, we did a similar exercise to generate the design space. And this is what we obtained. Again, the cycle we conducted was down here, the yellow, the orange circle, whereas the most efficient cycle would've been somewhere here at a shelf temperature of 20 C, and a chamber pressure of 100, 110 millitorr.

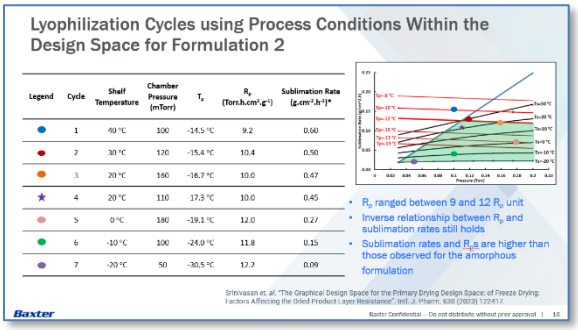

We did the same thing here wherein we looked at a series of process parameters within this design space and then connected that many cycles and then generated that many Rp data and the sublimation data. Again, the same trend of an inverse relationship between the Rp and the sublimation rates still held good with this particular formulation. In addition, if you look at the Rp values by themselves for this particular formulation, the highest Rp we observed was 12.2, but the lowest was 9.2.

For the sucrose formulation, if you remember, the range was between four and 13 or seven and 13, depending on if you take that cycle that was outside of the design space into consideration or not.

But for this particular formulation, the Rp was much tighter than it was for the sucrose formulation. And the sublimation rates were a lot higher as you would imagine, because the shelf temperatures were a little higher as well.

There is a question that came through. Slide number 16, why the values of pressure and shelf doesn't match with the correspondent mass flow? Again, there are differences, same differences like I told you previously with respect to how the design space was calculated using a constant Rp, and then how these different cycles span out with respect to varying Rps within the same cycle. So that is the one that gives rise to different sublimation rates, the absorbed versus the calculator. I hope that answered the question. And then we already went over this data.

And then the reason why I conducted that particular cycle for the sucrose formulation, which was outside of the green zone at minus 10 C and a hundred millitorr, was were the data observed for that formulation using those conditions, with the mannitol formulation. Because mannitol, since it's crystalline, you have the ability to be able to conduct your shelf cycles at more aggressive conditions than for sucrose. I only had a couple of data points that were direct comparison of the two formulations. So one of them was minus 10 C at a hundred millitorr.

For formulation one, which was sucrose formulation, the product temperature was much lower than for the crystalline formulation. But then if you compare the Rps, you can see a drastic difference. For the sucrose formulation, it was four 4.0, which was much lower than 11.8 that we observed for the mannitol formulation. So Rp is dependent on the formulation, and we already showed in the previous slides that Rp varies depending on what process parameters you use within the design space of given formulation.

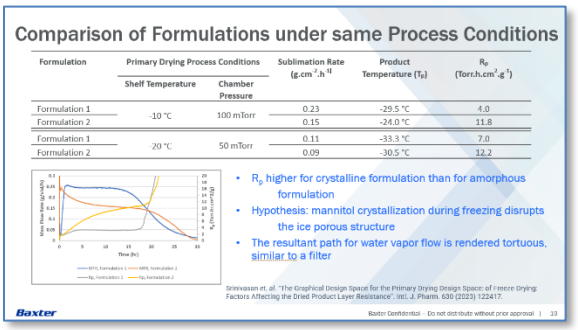

Just to compare the process data with respect to the two formulations for another cycle conditions, which was minus 20 C and 50 millitorr, again, you see a big difference in the Rp data for the two cycles.

And just to pictorially show you how the differences manifest, with respect to the two formulations. The gray line here is the Rp graph Rp line, for the sucrose formulation. As you can see, it is pretty constant throughout as soon as sublimation starts. When the shelf temperature reaches the temperature set

point, from there on until the end of primary drying, it is relatively constant. The Rp is constant. And then it increases sharply at the end of primary drying.

Whereas if you look at the same Rp graph, for formulation two, for the mannitol formulation, the Rp increases steadily until the end of primary drying, and then it increases sharply. So, there is a big difference in the behavior of the two formulations with respect to the product resistance. And then you see a similar difference in the mass flow rate data as well.

For the sucrose formulation, since the Rp is constant, the mass flow rate is also relatively constant, until at the end of primary drain when it declines sharply. Whereas for the mannitol formulation, there is a steady decrease in the mass flow rate until the end of primary drying.

What is the reason behind the mannitol formulation or the crystalline formulation exhibiting a higher Rp than the amorphous formulation? Our hypothesis is that in the crystalline formulation, mannitol obviously crystallizes. We also had an enabling step just to ensure that all the mannitol crystallizes. So, the customization of mannitol somehow disrupts the freezing behavior and the ice crystallization as well, and the ice porous structure. So that results in water vapor during sublimation, the water vapor, it encounters a tortuous path for sublimation in the crystalline formulation. Whereas in the amorphous formulation, it's only the ice that crystallizes and everything. All other components remain amorphous. Probably the ice path, the water vapor path is more straightforward than it is for a crystalline formulation is what we think is happening.

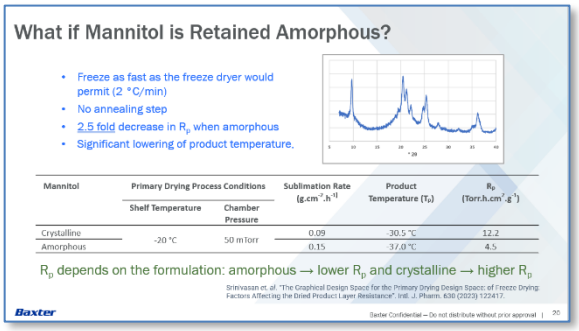

So now we know we have some data with respect to the amorphous in the crystalline formulation and the actual behavior of the two formulations with respect to the product resistance. What is it that we can change within the formulation? But, not changing the formulation, keep the formulations the same, but then change the process parameters, or change the nature of your components so that you're able to flip the amorphous formulation into crystalline or crystalline into amorphous nature.

With sucrose, you cannot make it crystallized, whereas with mannitol you can make it not crystallized during the freezing step. So that's what we exactly did. We attempted to retain mannitol amorphous by either flash freezing in liquid nitrogen, or conducting the freezing step as fast as the dryer is capable of doing. For our freeze-dryer, that freezing rate is about two degrees C per minute.

So, for this particular cycle, which I used the fast freezing step, instead of the flash freezing with liquid nitrogen, this is what we obtained. I did x-ray powder [inaudible 00:31:53] to see if mannitol remained amorphous or not.

For most part, it remained amorphous. We also saw a little bit of mannitol crystallizing, because presumably to see a minute is not fast enough to prevent mannitol crystallization. So regardless, we went ahead and conducted primary drying and secondary drying with this amorphous mannitol formulation.

And here we are comparing the two data of the mannitol formulation, but one crystalline and one amorphous, the other amorphous. Same shelf temperature and chamber pressure. The sublimation rates are different here in this case. For the crystalline formulation, the sublimation rate is low. It is 0.09 for these particular parameters that we used. And for the amorphous formulation, it was much higher.

And the product temperatures flipped in the sense that for the crystalline formulation it was much higher, whereas for the amorphous formulation it was lower.

And then if you look at the Rp, we were surprised with this result, for the crystalline mannitol, it was 12.2, whereas for the amorphous mannitol it was 4.5. So the amorphous mannitol behaved similar to the sucrose formulation.

That tells you that this lower Rp is probably unique to the amorphous nature of the formulation. And the crystallinity of your excipient affects the Rp directly and it increases it during sublimation.

Moving on to the mixed system, which contained both sucrose and mannitol, we did a similar series of cycles within the design space. But then if you look at the Rps, the Rps are even tighter for this particular formulation than it was for the crystalline formulation. It ranged between seven and nine, which are definitely lower than we had observed for the crystalline mannitol formulation. So the mixed system presumably behaves similar to sucrose, so more closer to sucrose than to mannitol is the bottom line here.

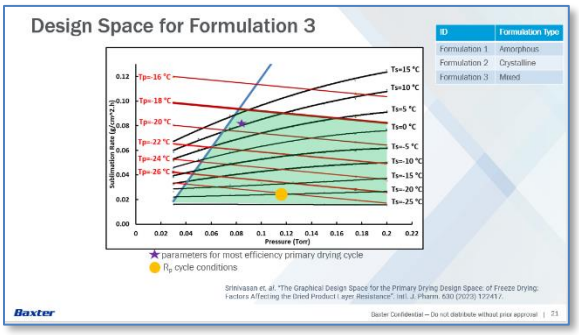

If you were to compare, again, the Rps of the three formulations and also side-by-side comparison here, and also the morphous mannitol here, you can see clearly for the sucrose formulation, like I said previously, the Rp remains the same during sublimation. And for the amorphous mannitol formulation, it remained about the same. Since there was a little bit of mannitol that had crystallized, that probably impacted the Rp in the sense that it increased, slightly, during sublimation but not as big a deal as crystalline mannitol.

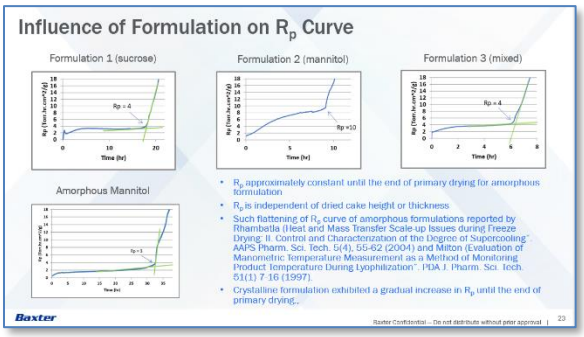

So, this kind of constant Rp for amorphous formulations is not new. It has been absorbed previously and has been reported in the literature. So, you can look at these two articles, that suggests that the sucrose behavior is somewhat expected, but the crystalline formulation behavior is and the mannitol formulation behavior were somewhat surprising to us.

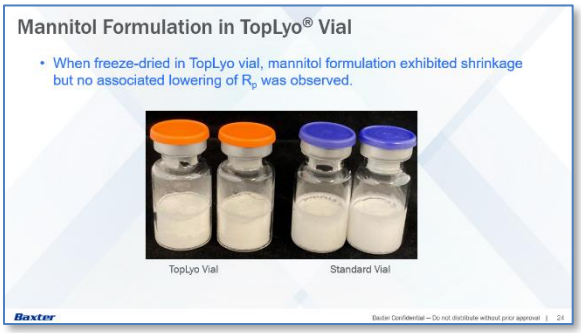

Oh yeah, the other experiment that we performed was the TopLyo. So again, we want to maintain mannitol crystalline. So we already answered if your crystalline component remains amorphous, it behaves similar to an amorphous formulation in lowering the Rp. So what if in amorphous formulations, with sucrose formulations especially you observe shrinkage, it's very common. So what if the shrinkage is the one that's responsible for lowering the Rp? Obviously by shrinking, what you basically do is to open up pathways along the sides of the vial. So that probably provides additional pathways for the water vapor to escape during sublimation. Maybe that's why the Rp is lower.

In order to probe that hypothesis, what we did was, we used the mannitol formulation, crystallized it during the freezing step, but used at TopLyo vial, instead of your standard short vial. So TopLyo vial, as you know, it has the hydrophobic coating that results in the cake, the freeze-dried solid, separating from the wall vial, because of the shrinkage.

We wanted to see if that had an impact. So, we did this cycle using a TopLyo vial and this is what we observed. The orange capped vial on the left is the TopLyo vials, and the two vials on the right are the standard vials. We did observe shrinkage with respect to the formulation, the mannitol formulation, but what we did not observe was a lowering of the Rp. The Rp remained about the same.

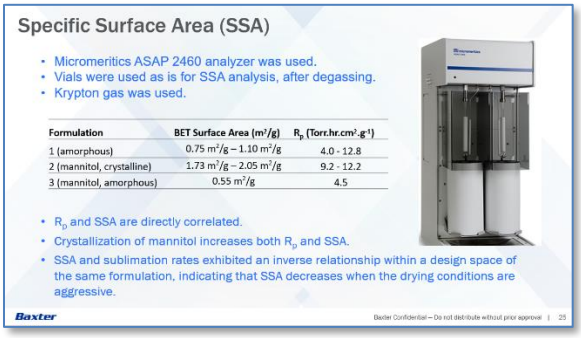

This implies that it is not the shrinkage that decreases the Rp. It's rather the crystallization of mannitol in the crystalline formulation that increases the Rp due to the tortuosity associated with the crystallization of the excipient itself and for the water vapor escape during sublimation.

We went ahead and characterized the free straight solids for surface areas using this instrument, the Micromeritics ASAP instrument. So, it has a dual chamber that enables us to characterize two samples at once. And we use the vial assets. We do not do any sample preparation.

This is just a summary of all the data that we obtained for this particular analysis, specific surface area analysis. The bottom line is the Rp, so if you compare the BET surface area versus Rp, for the sucrose formulation, the lower the Rp, the lower the surface area. So, there is a direct correlation between the Rp and the surface area.

And for the crystalline formulation, formulation two, the surface areas are higher than then those are for the amorphous formulation, but that's also very apparent. There is an inverse relationship between the sublimation rates and the surface areas. And then for the amorphous formulation, the surface area was similar to that of the sucrose formulation because the Rp resembled the amorphous formulation Rp.

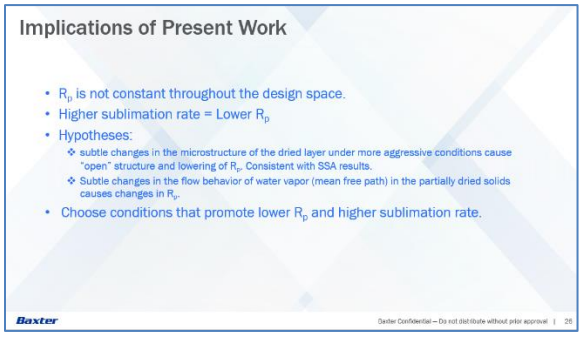

In terms of implications of this study, we observed that Rp is not constant for the same formulation. The Rp is not constant within the design space. It varies based on the process parameters you use. And the higher the sublimation rates, that is the higher the shelf temperatures that you use for your cycle, the lower the Rp.

We have a couple of hypotheses for these observations. The reason why for more aggressive cycles the Rp is lower is because probably it has to do with the microstructure. With aggressive cycles, you are probably cause of the highest sublimation rates are causing more of an open structure and that lowers the Rp. And this is consistent with the surface area result as well.

And then the reason why you see a difference in the Rp with the Rps within the same formulation could be because the flow behavior during sublimation of the water vapor changes probably and changing between molecular flow to a viscous flow that results in different changing the Rps.

These are our hypothesis. We need to probe these further. But for now, these are our observations. So it would be prudent for you to choose cycle parameters that are closer to the apex of the collapsed temperature and the equipment capability limit curve, but then staying within, or below, under the apex because you do have edge vials that are much warmer than the center vials. But then choosing conditions that provide the maximum sublimation rate is going to be your most efficient cycle, because it's going to be your fastest cycle.

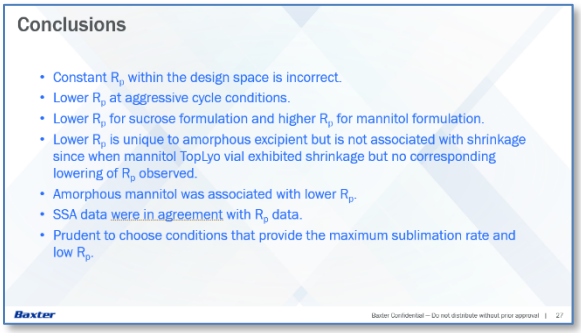

In terms of conclusions, what we set out to do, we were able to achieve that because we wanted to probe if Rp remained the same throughout the design space and it turned out to be not true. And then Rp was dependent on the cycle parameters obviously. But then for aggressive cycles, Rp tended to be lower than for more conservative cycles. And then Rp was much lower for the amorphous formulation than it was for the crystalline formulation.

I went over all these already, so in the interest of time, I'm not going to go over every single point. We are right at about time, but there were a few questions that already came through and I wanted to take this time to address that.

But then before I do that, I wanted to acknowledge Greg Sasha and Steve Nail, they were involved in this project, and then the Baxter BioPharma solutions, the R&D group.

And just so you know, if you're interested in a position in our group, we are hiring. Please feel free to reach out to me. My email is in the bottom and Millrock for this opportunity, they have a much wider audience and I'm glad that they reach out to me for this webinar. And thank you all for your attention.

I'm going to go back to the questions that are already posted and then, Brian, maybe you can help me with any new questions or questions that I'm not able to see here.

*For economical alternatives to TDLAS please refer to studies attached.

International Journal of Pharmaceutics 643 (2023) 123285

Contents lists available at ScienceDirect

International Journal of Pharmaceutics

journal homepage: www.elsevier.com/locate/ijpharm

Lyophilization cycle design for highly concentrated protein formulations supported by micro freeze-dryer and heat flux sensor

Marco Carfagna [a,b], Monica Rosa [a], Andrea Hawe [a,*], Wolfgang Frieß [b]

[a] Coriolis Pharma Research GmbH, Fraunhoferstrasse 18 b, 82152 Martinsried, Germany
[b] Department of Pharmacy, Pharmaceutical Technology and Biopharmaceutics, Butenandtstrasse 5, Ludwig-Maximilians-Universitaet München, D-81377 Munich, Germany

ARTICLE INFO

Keywords:
High-concentration protein formulations
Freeze-drying
MicroFD
QbD
Heat flux sensor

ABSTRACT

High-concentration protein formulations (HCPFs) represent a common strategy and freeze-drying can mitigate the stability challenges of HCPFs. In general, an in-depth characterization of the lyophilization process is essential to not impair the product quality by inappropriate process parameters. The aim of this study was to create a primary drying design space for lyophilized HCPFs by utilizing the heat flux sensor (HFS) integrated in a MicroFD with a minimum number of cycles and product vials. All the necessary data to obtain the design space were determined starting from only two lyophilization cycles, each holding 19 vials. The vial heat transfer coefficient (Kv) was determined by the HFS and compared to gravimetric values. The results indicate a consistant offset between the HFS and the gravimetry based values for annealed samples with higher protein content. This work highlights a possibility of integrating new technologies, the HFS and the MicroFD to generate a design space for lyophilization of HCPFs, which enables to implement a QbD approach at minimal material and time investment.

1. Introduction

The subcutaneous administration of biopharmaceuticals represents a valuable alternative compared to the intravenous route, especially for chronic diseases (Ward and Matejtschuk, 2019). In fact, it presents the advantages of home medication in addition to a higher patient compliance. The injectable volume is usually in the range of 1–2 ml to avoid pain for the patients and difficulties in administration (Cilurzo et al., 2011; Narasimhan et al., 2012). In the case of antibodies this may lead to formulations with high protein concentration between 100 and 200 mg/ml (Shire et al., 2004; Ward and Matejtschuk, 2019). At such high concentrations, challenges of increased viscosity, limited solubility and reduced protein stability arise (Shire et al., 2004). In the case of limited protein stability, converting the liquid formulation into a lyophilizate can be an appropriate route of choice (Kasper and Friess, 2011).

Lyophilization of high-concentration protein formulations (HCPFs) brings multiple challenges. The product resistance to the sublimation flow is usually higher and this can result in longer drying times (Garidel and Presser, 2019; Tang and Pikal, 2004). On the other hand, the collapse temperature increases with higher protein concentrations (Colandene et al., 2007), which allow a drying under harsher conditions. Overall, it is important to find a good balance in reducing the primary drying time at higher temperatures without affecting product quality (Butreddy et al., 2020; Fissore et al., 2011). Especially considering that the overall cost of a HCPF batch can be extremely high, i.e., 30,000 lyophilized vials filled with 100 mg/ml recombinant protein value on average ca. $ 1.5 million (Cullen et al., 2022). The key fluxes governing the lyophilization process are the heat (Q), received by the vial, and the mass of sublimed water (J_w) which are both indirectly regulated by the temperature of the shelf, the circulating shelf fluid resp. (T_{fluid}) and the chamber pressure (P_c) (Scutellà et al., 2018). To mathematically describe the relation between these fluxes (Q and J_w) and the related input parameters (T_{fluid} and P_c), the vial heat transfer coefficient (K_v) and the product resistance (R_p) were introduced (Giordano et al., 2011; Pikal et al., 1984). Both are essential elements of the Quality by Design (QbD) approach in lyophilization and for a scientific process transfer (Kawasaki et al., 2019). K_v represents the impact of the vial and equipment on Q and depends mainly on P_c and position of the vial within the dryer (Hibler et al., 2012; Pikal et al., 1984). R_p depicts the impact of the formulation on J_w and is affected by the freezing conditions and the drying progression (Pikal et al., 1984; Pisano et al., 2013). The most reliable and classical way to obtain K_v is the gravimetric method based on determination of water loss after certain sublimation

* Corresponding author.
E-mail address: Andrea.Hawe@coriolis-pharma.com (A. Hawe).

https://doi.org/10.1016/j.ijpharm.2023.123285
Received 13 April 2023; Received in revised form 11 July 2023; Accepted 30 July 2023
Available online 31 July 2023

Abbreviations and Nomenclature

A_v	cross sectional area of vial (m^2)
BSA	bovine serum albumin
ΔH_s	sublimation heat (J kg^{-1})
Δm	sublimed mass (kg)
Δt	considered drying time (s)
F	1-step freezing
FD	freeze-dryer
grav	Gravimetric
HCPF	high-concentration protein formulation
HFS	heat flux sensor
J_w	sublimation flux (kg m^{-2} s^{-1})
K_v	vial heat transfer coefficient (W m^{-2} K^{-1})
$K_{v\ grav}$	vial heat transfer coefficient (W m^{-2} K^{-1}) gravimetric-based
$K_{v\ HFS}$	vial heat transfer coefficient (W m^{-2} K^{-1}) HFS-based
k_{frozen}	thermal conductivity of the frozen layer ($W{\cdot}m^{-1}{\cdot}K^{-1}$)
L_{frozen}	thickness of frozen layer (m)
l_v	average distance between vial bottom to the shelf (m^{-1})
λ_0	thermal conductivity of the gas at ambient pressure ($W{\cdot}m^{-1}{\cdot}K^{-1}$)
P_c	chamber pressure (Pa)
PD	primary drying
P_i	pressure at the sublimating interface (Pa)
PVDF	polyvinylidene difluoride
Q	heat received by a vial (W m^{-2})
QbD	Quality by Design
Q_{HFS}	heat measured from heat flux sensor (W m^{-2})
RH	relative humidity
R_p	product resistance (m s^{-1})
ρ_{dried}	apparent density of the dried product (kg m^{-3})
ρ_{frozen}	density of the frozen product (kg m^{-3})
t	time (s)
T_{fluid}	temperature of fluid circulating in the shelf (°C)
T_i	temperature at the sublimating interface (°C)
T_p	product temperature (°C)
$T_{shelf\ surface}$	shelf surface temperature as measured by heat flux sensor (°C)
T_c	collapse temperature (°C)
V_{fill}	filling volume (ml)
2F	2-step freezing
2FA	2-step freezing and annealing
3-PE	3-pressure experiment

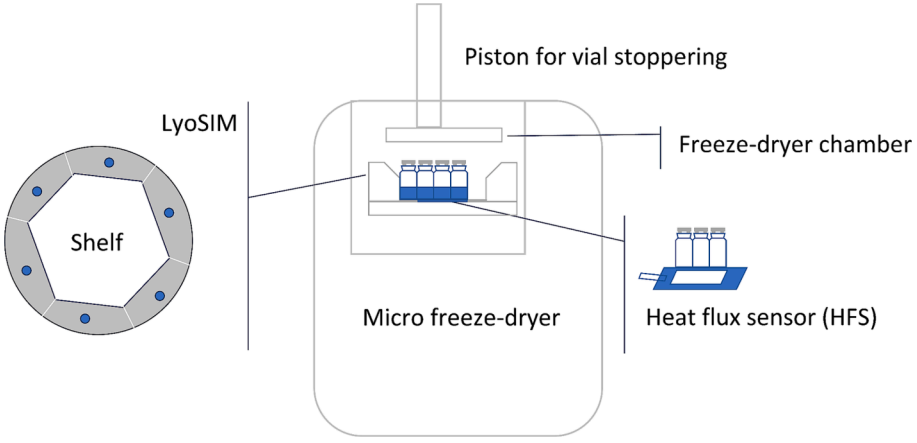

Fig. 1. Schematic representation of the MicroFD and key components. Top-view of the LyoSIM is shown.

times during primary drying. This approach enables differentiation between center or edge vials on different shelves. Based on K_v, R_p can be obtained and the evolution of the dried layer thickness can be followed (Kuu et al., 2011). The gravimetric method has some limitations. It requires the abortion of the process during primary drying, it is rather time-consuming, and results are not available in real-time for process monitoring and control (Bosca et al., 2014). Another option for K_v determination is pressure rise test (PRT) methods, where the chamber pressure increases due to isolation between the lyophilization chamber and the condenser for a variable time (3–30 s), which feeds different algorithms based on the specific methods. PRT requires a fast-closing valve to isolate the lyophilization chamber, which is not available for all freeze-dryers. Furthermore, PRT may offer unreliable results for high solid content amorphous products due to re-adsorption effects (total solid content >150 mg/ml) (Gieseler et al., 2007). An additional method for K_v determination is tunable diode laser absorption spectroscopy (TDLAS) that measures the flow and composition of the gas in the duct connecting drying chamber and the condenser. TDLAS is costly and can only be *retro*-fitted in freeze-dryers with a duct between chamber and condenser. PRT and TDLAS provide an average K_v, for the whole batch and cannot differentiate between edge and center vials (Kauppinen, 2015).

Recently, heat flux sensors (HFSs) have been evaluated as a PAT tool to monitor the overall process in-line (Moino et al., 2021; Vollrath et al., 2019). Published studies highlighted the capabilities of HFS in detecting the end of ice crystal growth during the freezing and as the end point in primary drying (Moino et al., 2021; Vollrath et al., 2019).

It is of major interest to gain process knowledge transferable to manufacturing equipment to mitigate the risk for commercial batches. In this regard, we have previously assessed the feasibility by obtaining key process parameters and consequently in creating a design space for a placebo formulation by using an HFS in a standard lab-scale freeze-dryer (Carfagna et al., 2020). More recently, a miniaturized freeze-dryer equipped with HFS and has been introduced onto the market. As suggested by the commercial name, MicroFD, the equipment has a smaller size. The shelf can accommodate a limited number of vials (e.g., a maximum of 19 6R vials) with the aim of saving material and efforts during lyophilization cycle development. Besides other standard components, this equipment includes the HFS and a component named LyoSIM which can emulate different heat transfer scenarios (Fig. 1).

As HCPFs present many technical challenges from manufacturability to stability, obtaining in-depth knowledge about the lyophilization process with a minimum amount of material and time is of high interest. In this context, the combined use of the HFS and MicroFD to generate and select a valid design space for HCPF have been explored.

Therefore, the aim of our study was to verify if HFS/MicroFD can be applied for HCPF and to confirm their potential for design space creation. To this end, we determined K_v and R_p of HCPF in a MicroFD. Subsequently, we generated a design space for the primary drying process and confirmed its validity experimentally by estimation of primary drying time, product temperature profile whilst additionally considering cake appearance and water content.

2. Materials and methods

2.1. Formulations and primary packaging

Experiments were carried out with 50 and 150 mg/ml solution of Bovine Serum Albumin (BSA) (Sigma-Aldrich, Munich, Germany) with 10 % w/v sucrose (Ph. Eur. grade; Merck, Darmstadt, Germany) in 10 mM sodium phosphate buffer pH 7.4. The BSA concentration of both formulations was checked after filtration through 0.22 μm PVDF membrane filters (Merck, Darmstadt, Germany) by using a Nanodrop 2000 UV photometer (Thermo Fisher Scientific, Wilmington, USA). 2.6 ml solution were filled in 6R TopLyo glass vials (Schott, Müllheim-Hügelheim, Germany) unless differently specified. The vials were partially closed with 20-mm bromobutyl single vent lyophilization stoppers (Westar RS, FluoroTec B2-40 coating; West, Eschweiler, Germany).

2.2. Freeze-drying equipment and heat flux sensor (HFS)

19 vials were processed in a 0.07 m^2 shelf area MicroFD (Millrock Technology, Kingston, NY) equipped with an HFS located at the center of the shelf. Vials were surrounded by the LyoSIM ring, the temperature of which can be regulated with an offset to T_p (range ± 15 °C) or between −60 and +60 °C independently of T_p (Carfagna et al., 2022; Goldman et al., 2019). This component is a temperature-regulated ring composed of 6 metallic blocks on the edge of the shelf surface. The size of the LyoSIM blocks is adjusted to the vial diameter which results in a hexagonal array of vials when the full capacity is reached. Thereby, the wall of vials at the edge come into contact with the blocks (Fig. 1). In this study, the LyoSIM temperature had an offset to the center vial T_p of 0 °C during freezing and −15 °C during drying. These parameters were selected based on previous work (Carfagna et al., 2022). Pressure was controlled by a capacitance manometer and monitored in addition with a Pirani gauge. Product temperature was measured by T-type copper-constantan thermocouples in combination with thermocouple holders (Millrock Technology, Kingston, NY).

2.3. Determination of K_v and R_p and their mathematical description

The following freezing protocols were evaluated:

- 1-step freezing (F) by ramping down to −50 °C at 1 °C/min
- 2-step freezing (2F) by equilibrating the samples at −3 °C for 60 min followed by ramping down to −50 °C at 1 °C/min
- 2-step freezing and annealing (2FA) by equilibrating the samples at −3 °C for 60 min followed by ramping down to −50 °C at 1 °C/min followed by a ramp to −10 °C at 1 °C/min, a 260 min hold at −10 °C followed another ramp to −50 °C at 1 °C/min

For each protocol, the final freezing temperature was held for at least 2 h. Primary drying was conducted at 5 Pa and −20 °C as T_{fluid}. Water loss (Δm) was measured by weighing all 19 filled vials placed in the MicroFD before the start of the process and after approximately 10 h of primary drying on an analytical balance (Genius ME – Sartorius, Gottingen, Germany). In this time frame, T_p is consistently reliable because the thermocouple keeps contact with the material as the drying is prematurely stopped. K_v grav and K_v HFS were calculated according to the following equations:

$$K_{vgrav} = \frac{\Delta m \Delta H_s}{A_v \int_0^{\Delta t} (T_{fluid} - T_p) dt} \quad (1)$$

where ΔH_s is the sublimation heat of ice, and A_v is the cross-sectional area of the vial.

The HFS-based K_v (K_v HFS) is related to the sensor readout (Q_{HFS}) as by the following equation:

$$K_{vHFS} = \frac{Q_{HFS}}{(T_{shelfsurface} - T_p)} \quad (2)$$

where $T_{shelf\ surface}$ is the temperature of the shelf surface as measured from the built-in thermocouple of the HFS, and T_p is the product temperature measured at the vial bottom from the thermocouple. T_{fluid} is the shelf fluid temperature set in the MicroFD. To generate K_v at three different chamber pressures a 3-pressure experiment (3PE) was performed for the 150 mg/ml BSA formulation. A 2FA protocol with annealing at −10 °C was followed to a temperature decrease of T_{fluid} until −50 °C. For primary drying the shelf temperature was set at −20 °C and chamber pressure was initially set at 5 Pa, then increased at 11 Pa and finally at 16 Pa. The LyoSIM was set at −15 °C offset compared to T_p, as in the single pressure experiments. For the comparison between K_v grav and K_v HFS, the average of gravimetric values was considered. More specifically, the data from vials placed above the HFS, were included in the calculation, with the exception of the one containing the thermocouple.

The product resistance (R_p) was obtained by the following equation:

$$R_p = \frac{(P_i - P_c)}{J_w} \quad (3)$$

where J_w is the sublimation flux as obtained from Eqs. (4)–(5), P_i is the pressure at the sublimating interface determined from the Goff-Gratch equation and, T_i, the temperature at the sublimating interface that can be approximated to T_p.

$$Q = K_v (T_{fluid} - T_p) \quad (4)$$

$$J_w = \frac{Q}{\Delta H_s} \quad (5)$$

K_v and R_p were mathematically described by non-linear fitting by the following equations:

$$K_v = A_{Kv} + \frac{B_{Kv} P_C}{1 + l_v \frac{B_{Kv}}{\lambda_0} P_C} \quad (6)$$

$$R_p = R_{p0} + \frac{A_{Rp} L_{dried}}{1 + B_{Rp} L_{dried}} \quad (7)$$

Details on equations coefficients and physical constant can be found in previous publications (Carfagna et al., 2022; Fissore et al., 2012). A_{Kv}, B_{Kv} are obtained from the best fit of K_v vs. P_c variation while R_{p0}, A_{Rp} and B_{Rp} from the best fit of R_p vs. dried layer (L_{dried}) evolution.

2.4. Analysis of collapse temperature(T_c)

The collapse temperature (T_c) of the formulations was analyzed with a Linkam microscope equipped with an FDCS 196 freeze-drying stage (Linkam Scientific Instruments, Surrey, UK). 2 μl of formulation were pipetted on a quartz crucible and a cover slip was placed above the droplet with a 25-μm spacer. The sample was frozen at 1 K/min to −50 °C. Afterwards, two alternative protocols were executed:

Table 1
Parameters for the verification freeze-drying cycle.

No.	Step	Time [hh:mm:ss]	Cumulative Process Time [hh:mm:ss]	T_{fluid} [°C]	P_c [Pa]	Cooling/heating rate [°C/min]
1	Loading	00:10:00	–	20	100,000	
2	Freezing	00:46:00	00:56:00	−3	100,000	0.50
3		01:00:00	01:56:00	−3	100,000	
4		00:47:00	02:43:00	−50	100,000	1.00
5		02:00:00	04:43:00	−50	100,000	
6		00:40:00	05:23:00	−10	100,000	0.50
7		06:00:00	11:23:00	−10	100,000	
8		00:40:00	12:03:00	−50	100,000	0.50
9		02:00:00	14:03:00	−50	100,000	
10	Primary drying	00:15:00	14:18:00	−50	11	
11		02:40:00	16:58:00	30	11	0.50
12		06:24:00	23:22:00	30	11	
13	Secondary drying	06:00:00	29:22:00	30	11	

a) vacuum was applied to start the drying
b) sample was annealed to −10 °C, cooled again at −50 °C with holding times in both cases of 10 min and then vacuum applied

Once the vacuum level reached 10 Pa, the sample was heated at 1 K/min to −40 °C and the sample was kept for 10 min at that temperature to obtain a suitable dried layer. The sample was heated to 5 °C using a heating rate of 1 °C/min and images were taken every second. Collapse temperature of the frozen solution was determined from the appearance of translucent dots or fissures behind the ice sublimation interface.

2.5. Design space creation and verification of the optimized cycle

A design space for each formulation (50 and 150 mg/ml) was created based on the mathematical model proposed by Velardi and Barresi (Velardi and Barresi, 2008) for the freezing protocols 2F and 2FA. The algorithm was applied to estimate the evolution of dried material thickness, temperature at the sublimating interface (T_i) and primary drying time. In particular, the evolution of the frozen layer (L_{frozen}), reciprocal of the dried layer, is calculated based on the sublimation flux (Eq. (3)):

$$\frac{dL_{frozen}}{dt} = \frac{1}{\rho_{frozen} - \rho_{dried}} \frac{(P_i - P_c)}{R_p} \tag{8}$$

where ρ_{frozen} and ρ_{dried} indicate the density of the frozen and the apparent density of the dried product respectively. The relation between T_p, T_{fluid} and T_i is expressed as

$$T_p = T_{fluid} - \frac{1}{K_v} \frac{(T_{fluid} - T_i)}{\left(\frac{1}{K_v} + \frac{L_{frozen}}{k_{frozen}}\right)} \tag{9}$$

where k_{frozen} is the thermal conductivity of the frozen layer. Based on this equation and that all heat received by the frozen product is used for sublimation (Eq. (5)) and pseudo-stationary conditions that allow process evolution to be described as in Eq. (8), at the sublimating interface, the energy balance can be written as:

$$\frac{(P_i - P_c)}{R_p} \Delta H_s = T_{fluid} - \frac{(T_{fluid} - T_i)}{\left(\frac{1}{K_v} + \frac{L_{frozen}}{k_{frozen}}\right)} \tag{10}$$

The optimized verification cycle parameters are summarized in Table 1. The transition from primary to secondary drying was defined in advance and not on the comparative pressure Pirani/Capacitance. Time

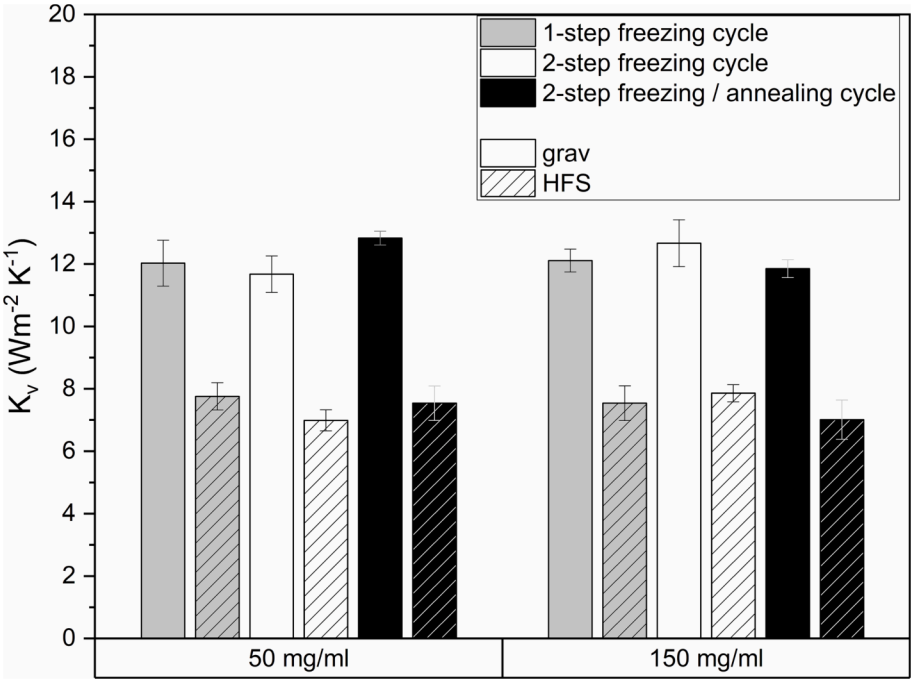

Fig. 2. Comparison of gravimetric and HFS based Kv for 50 and 150 mg/ml BSA formulation for three different freezing protocols.

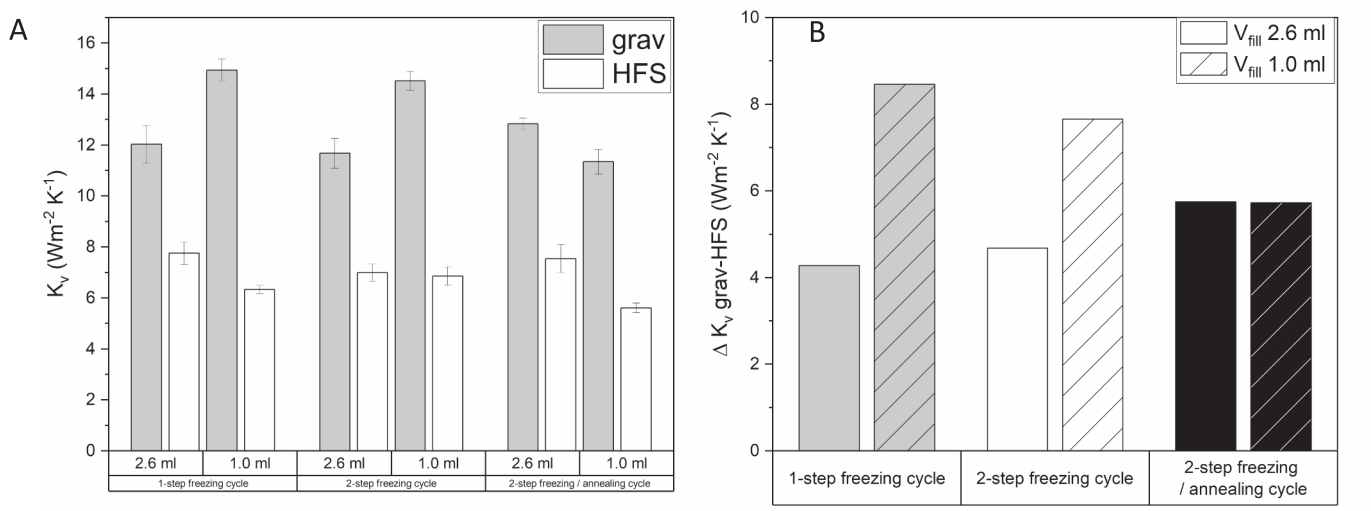

Fig. 3. Comparison of Kv grav and Kv HFS results by considering three freezing protocols and two filling volumes (A) Focus on the difference between gravimetric and HFS-based values (B) – 50 mg/ml BSA formulation.

of desorption in secondary drying was set to 6 h.

2.6. Optical evaluation of the freeze-dried product

The freeze-dried cakes were visually evaluated for compactness, contact to walls of vial, shape, color and overall appearance. Furthermore, photos were taken. Scanning electron microscope (SEM) images were generated with a bench top SEM (Phenom-World B.V., Eindhoven, The Netherlands) after transferring samples in a glove box under controlled humidity conditions (<10% relative humidity) and preparing a slice from the cross section of the center part of the lyophilizates.

2.7. Residual moisture analysis

The residual moisture content of the lyophilizates was analyzed by Karl Fischer titration with an Aqua 40.00 (Analytik Jena, Jena, Germany) using a head space module. The samples were prepared in a glovebox at ≤10% relative humidity. Approximately 50–80 mg sample was weighed into an empty 2R vial and stoppered. Blank values were obtained from empty vials. The vials were heated to 120 °C in the oven connected to the reaction vessel via a tubing system. The titration occurred until water evaporation was no longer detectable.

2.8. Data analysis

Throughout the manuscript, if not stated differently, values are given as mean ± standard deviation. Gravimetric K_v was calculated on n = 6 and Karl Fischer results are based on n = 3.

3. Results and discussion

3.1. HFS-based parameters for HCPF

The heat transfer coefficient K_v is a key factor to consider when designing freeze-drying cycles. It is used to predict the product temperature and therefore the primary drying time. We investigated the impact of the freezing protocol on the determination of HFS-based and gravimetric K_v (Fig. 2). It was deemed appropriate to incorporate different freezing protocols for two main reasons. Firstly, we wanted to assess the constant corrective factor between gravimetric and HFS-based. Secondly, we sought to also evaluate whether it was possible to screen the freezing protocol ad-hoc for a product, with the aim of determining drying time/process time, T_p and design space before the freeze-dying cycle is potentially transferred to another equipment. Additionally, the knowledge of the necessary process parameters and applicable ranges in the freeze-dryer where the product will be transferred will minimize the risks of the transfer/scale-up. More specifically, the 2F protocol with the −3 °C hold phase was included as a soak step so that all product vials were equilibrated before initiating the freezing to reduce vial-to-vial variability. The annealing phase in the 2FA protocol and the single-step freezing, the 1F protocol, were studied to understand the impact on product resistance when compared to the 2F protocol.

In accordance with the literature, the obtained K_v values were independent of the freezing protocol and the gravimetric K_v was consistently higher than the HFS-based K_v (Carfagna et al., 2022; Sane, 2016). The delta between HFS-based and gravimetric K_v was 4.5 $Wm^{-2}K^{-1}$ ± 0.3, except for the annealed 50 mg/ml BSA formulation. In this specific cycle, the cooling system showed a slower cooling rate post annealing with 0.4 vs. 1 °C/min (Figure S1) which, in combination with the delayed vacuum application, caused a higher T_p for the center vials and consequently a warmer LyoSIM. Therefore, the center vials were 5 °C warmer than edge vials in contact with the LyoSIM, and the resulting effect was a higher delta of 5.7 $Wm^{-2}K^{-1}$ for this specific cycle. The other experiments showed edge and center vials have a comparable temperature at a protein concentration of 150 mg/ml (Figure S1) confirming the optimal selection of LyoSIM setting. This aspect is highly relevant as the MicroFD presents the possibility to save time and material in the process design phase due to the reduced size and the availability of the HFS. These advantages can be exploited if the equipment can simulate the lab-scale freeze-dryer scenario and counteract atypical heat transfer, which is exacerbated in such a small freeze-dryer chamber. According to the manufacturer's claim, the LyoSIM simulates surrounding sublimating vials and acts as heat sink. Hence, edge vials should dry slower and be representative of center vials in a classic lab-scale equipment. A previous study examined the LyoSIM settings and the effect on the heat transfer coefficient (Carfagna et al., 2022). Based on a step-wise decrease of the offset compared to T_p, an optimal set-up of −15 °C was found. The current results confirmed that also for HCPFs the selected LyoSIM temperature offset is applicable.

To exclude any filling volume effect on K_v, additional experiments with a 1 ml instead of standard 2.6 ml filling volume were carried out for the 50 mg/ml BSA formulation. The T_p of the vials filled with less volume confirmed the finding that edge and center vials temperatures overlap (Figure S2). The delta between $K_{v\ grav}$ and $K_{v\ HFS}$ was higher with 1-ml fill volume in case of non-annealed samples (Fig. 3), whereas no difference could be observed for annealed products. This indicates

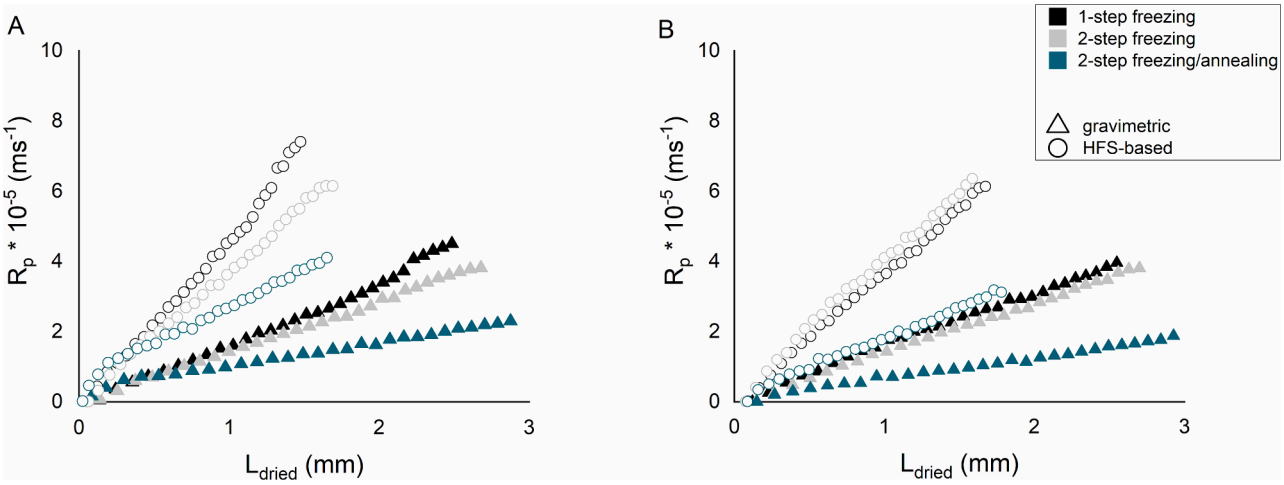

Fig. 4. R_p data for 50 mg/ml (A) and 150 mg/ml formulation (B) determined by using gravimetric and HFS-based Kv data determined for the different freezing protocols.

that a good batch homogeneity, which is improved by annealing (Nail et al., 2002; Tang and Pikal, 2004), is essential for K_v based modeling approaches, specifically when using $K_{v\ HFS}$. At higher concentration of 150 mg/ml the delta between the K_v techniques is less indicating a higher inter-vial homogeneity.

To verify the applicability of $K_{v\ HFS}$, the pressure dependence was investigated at three different P_c values. We performed a run covering three different P_c settings (3-PE) at 5, 11 and 16 Pa comparable to our previous work (Carfagna et al., 2022) and calculated the corresponding K_v HFS at each pressure (Carfagna et al., 2020). The obtained $K_{v\ HFS}$ values can be plotted against the P_c rendering the parameters A_{Kv} and B_{Kv} of a non-linear fit. While the previous gravimetric results were 8.7 $Wm^{-2}K^{-1}$ for A_{Kv} and 0.5 $Wm^{-2}K^{-1}$ Pa^{-1} for B_{Kv}, the current results HFS-based were 4.0 $Wm^{-2}K^{-1}$ for A_{Kv} and 0.5 $Wm^{-2}K^{-1}$ Pa^{-1} for B_{Kv}. The nonlinear fit is described by the parameter A_{Kv} that reflects well the highlighted offset of 4.5 $Wm^{-2}K^{-1}$ ± 0.3 and the B_{Kv} that expresses the same P_c dependency of gravimetric data. Based on the collected data, we consider this offset applicable in case of annealed HPCFs. The factors that mainly influence this offset are the filling volume (V_{fill}), the freezing protocol and, partially, the overall solid content. The first variable, V_{fill}, seems to have a bigger impact when small volumes are used where the K_v HFS is not able to detect the total heat received by the vial, specifically the portion of radial heat (Carfagna et al., 2022). At the same filling volume, annealing increases the difference between gravimetric and HFS based K_v. This can be explained considering that a lower R_p, and therefore a higher sublimation rate, is reflected in the K_v gravimetric, but not in the HFS-based K_v. This aspect is consistent with the same observation made on an amorphous excipient, which we previously published (Carfagna et al., 2022). However, this effect becomes less pronounced as the solid content increases. In case of 150 mg/ml despite the annealing effect, the amount of heat detected by the sensor, and consequently reflected by K_v HFS, is aligned to other freezing protocols and equal to 4.5 $Wm^{-2}K^{-1}$ ± 0.3. It is also interesting to note, that when V_{fill} is lower, annealing leads to higher batch homogeneity compared to other freezing protocols. This effect is beneficial an offset between the gravimetric and the HFS-based technique as in the case of higher solid content/higher V_{fill}.

After the focus on K_v, we evaluated R_p. As solid content affects product resistance, the HCPFs have a higher R_p value and hence a longer drying time. A common strategy to accelerate drying is to induce structural changes to the frozen matrix through the freezing protocol, mainly by annealing. The impact on specific surface area of the product is reflected in the drying time. The MicroFD allows a screening of freezing protocols and in this study, we exploited this potential. Overall, the heat transfer determinations impact considerably R_p calculations: HFS-based R_p is higher than the gravimetric R_p. The product resistance results are comparable in both formulations with higher values for 1F protocol for the lowest concentration. Our hypothesis is that this phenomenon is caused by increased inhomogeneity in the freezing phase. As expected, the obtained data confirm that annealing reduces the product resistance. More specifically, for both 50 and 150 mg/ml BSA, independently of the applied methodology, the annealing protocol results in a lower product resistance enabling faster drying compared to the one or two-step freezing approach, which appear equivalent in term of R_p (Fig. 4). Following the explanation highlighted in the K_v discussion, once we corrected the HFS-based K_v for the offset, we calculated the real R_p based on the "offset-corrected" K_v that is equivalent to the gravimetric K_v.

3.2. *Design space assessment – Impact of freezing protocols and protein content*

We used the combination of MicroFD and HFS for the first time to create a design space applied to HCPFs. This was achieved with only two lyophilization cycles, each of 19 vials that represent the full capacity of the MicroFD chamber for the studied primary packaging. The aim was to obtain a reliable procedure based on minimal experimental activities and material consumption. Therefore, the following steps were conceived:

a) K_v HFS-based
b) R_p estimation with K_v adjustment based on the determined offset
c) Determination of equipment constraints - in case of the MicroFD no equipment constrains were applied, due to the very low number of vials involved; determination of formulations constraints - in our case the T_c increases with protein concentration and annealing (T_c 50 mg/ml non-annealed: −16 °C, annealed: −14 °C; 150 mg/ml non-annealed: −13 °C, annealed: −10.5 °C – Figure S3)
d) Creation of design spaces for different R_p

The purpose of the design space is to visually depict which T_{fluid} and P_c can be applied without overcoming the collapse temperature (T_c) of the processed formulation. Product temperature varies during the drying process: as the thickness of the dried layer (L_{dried}) increases, resistance to sublimation flow changes. Therefore, when building the design space, we considered the product temperature at the sublimating interface (T_i) when ice thickness (L_{frozen}) is at its minimum. As drying is almost completed, this temperature is the maximum T_i reached for the selected inputs (T_{fluid} and P_c). The design spaces were created by mathematical simulations in a T_{fluid} range between −30 and +30 °C and

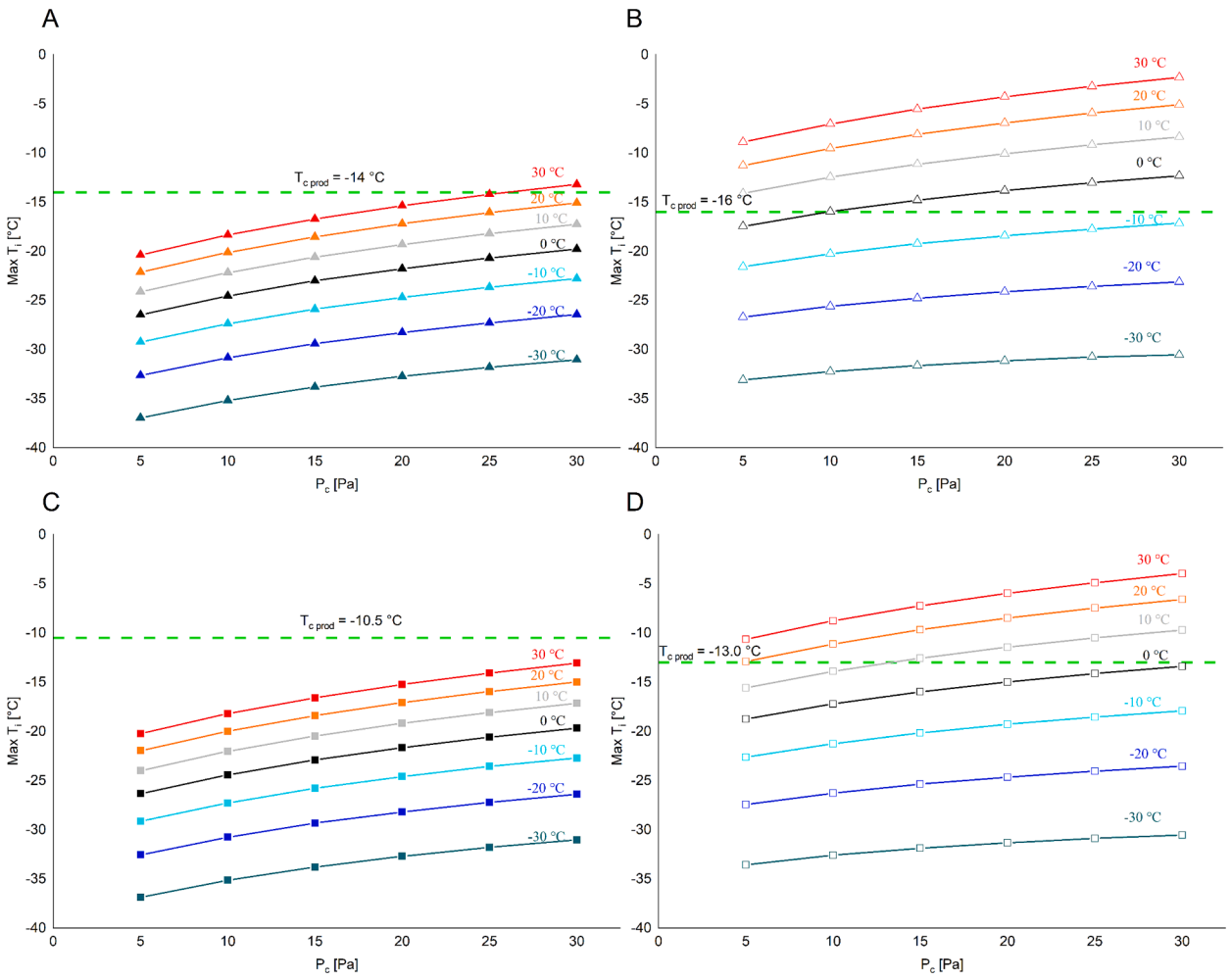

Fig. 5. Design spaces for different formulations and freezing options. The maximum values of T_i based on the input parameters (T_{fluid}, P_c) are plotted versus P_c. T_c (dashed line) is superimposed on the chart. Formulation 50 mg/ml 2-step freezing annealing (A) and 2-step freezing (B) and formulation 150 mg/ml 2-step freezing annealing (C) and 2-step freezing (D).

P_c from 5 to 30 Pa. The input variables were kept constant over the complete primary drying phase. The in-silico determination was based on the assumptions that all heat received by the frozen product is used for sublimation (Eq. (5)) and pseudo-stationary conditions that allow process evolution to be described as in Eq. (8). Additionally, considering that T_p can be described as function of T_i (Eq. (9)), the whole process can be summarized in Eq. (10). Hence, the model considering the K_v- P_c/R_p-dried layer description allows the determination of T_i, sublimation flow, and consequently Tp and drying time when L_{frozen} is equal to 0. Among the different options to present the design space, we chose to plot the max T_i versus the P_c. in order to highlight which combination T_{fluid}/P_c were part of the design space by imposing the formulation constraint (T_c) (Fig. 5). The first element of attention is the role of protein content that influences one of the design space borders, represented by the T_c. A second point is the influence of the different R_p on the shrinkage of the design space: a lower R_p, as in the case of annealing, creates a situation in which the freeze-dryer inputs (T_{fluid} and P_c.) have less influence on T_p and therefore can be set to higher values with a consequent shorter drying time. The collected data represent a valuable set of information that can accelerate the in-depth knowledge of the process and guide to a rational design of the freeze-drying cycle.

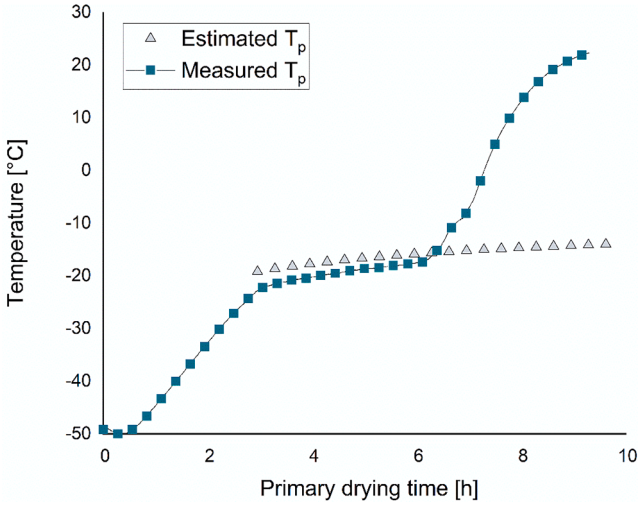

Fig. 6. Comparison between T_p measured during verification freeze-drying cycle and T_p estimated from our mathematical simulation.

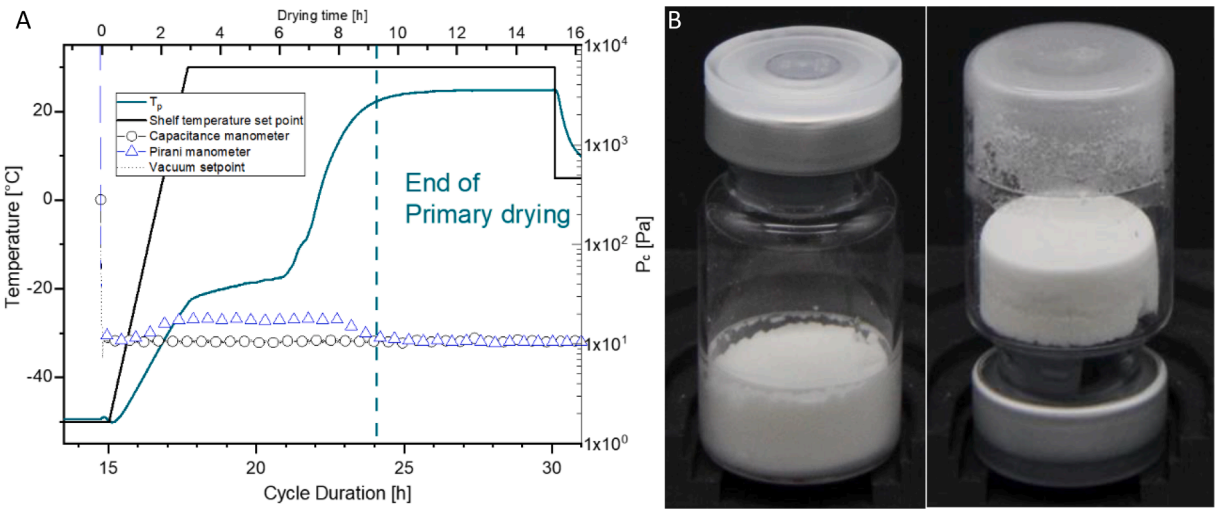

Fig. 7. Drying phases (primary/secondary drying) of the verification freeze-drying cycle [150 mg/ml BSA formulation – 2FA protocol] (A) - Cake appearance of exemplary final product from verification freeze-drying cycle (B).

3.3. Verification of the freeze-drying cyle selected based on the design space

The generated design spaces were taken as a basis to experimentally verify the predicted parameters for the 150 mg/ml formulation. The verification cycle was planned at the highest considered T_{fluid} of +30 °C and with a P_c of 11 Pa as midpoint of the tested range. According to our predictions, T_p should be in a range of −19.3 °C to −14 °C, respectively at the beginning and at the end of the primary drying (PD) holding phase respectively. The PD time was estimated in a range between 9.5 and 10.0 h based on K_v variability.

For the verification cycle, T_p was in a range of –22 °C and −15 °C at the beginning and until the thermocouple ceased to provide a reliable output, respectively (Fig. 6). The comparison between the measured and the estimated T_p was in good agreement. Additionally, the PD time equal to 9.3 h in the verification cycle, was consistent with the expected range based on the design space. In fact, it must be considered that the PD endpoint was experimentally determined by the alignment between the capacitance probe and the Pirani gauge (Fig. 7A) and an uncertainty of 12 min can be considered negligible due to the detection point and the limited amount of cycles performed.

The alignment between estimated and experimental results were corroborated by the characterization of the final lyophilized products. Macroscopically, pharmaceutically elegant cakes without signs of collapse were obtained with little vial to vial variability (Fig. 7B). SEM demonstrated a crust-like layer with the presence of pores and cracks homogenously-distributed at the top and a central part characterized by pores of approximately 50 μm in diameter (Fig. 8). The moisture level was low with 0.3 % ± 0.02 for center vials and 0.6 % ± 0.02 for edge vials. Thus, appearance and moisture level indicate that primary drying proceeded below T_c.

The verification was performed based on the data obtained in the Micro FD at minimal material and resource consumption considering the previously performed equipment characterization (Carfagna et al., 2022). The suitability of the combination of MicroFD and HFS to create a primary drying design space for HCPFs was confirmed based on product characteristics, product temperature profiles and primary drying duration. A general work flow would be:

a. Definition of the T_{fluid} in the target freeze-dryer involved in the transfer (indicated as FD02), starting from the data obtained in the MicroFD (indicated as FD01).

$$T_{fluidFD02} = \frac{K_{vFD02}\left(\frac{1}{K_{vFD02}} + \frac{L_{frozenFD01}}{k_{frozen}}\right)T_{pFD01} + T_{iFD01}}{K_{vFD02}\left(\frac{1}{K_{vFD02}} + \frac{L_{frozenFD01}}{k_{frozen}}\right) - 1} \quad (10)$$

considering the heat transfer coefficients of FD02 for edge and center vials and the previous Micro FD characterization (Carfagna et al., 2020).

b. Process simulation to set drying time and expected product thermal profile.

4. Conclusions

In summary, we present an approach to define a primary drying design space for lyophilization of high concentration protein formulations utilizing the HFS integrated into a MicroFD with only two lyophilization cycles, each of 19 vials. T_p and end of PD could be predicted well, and a collapse-free and low moisture content product was obtained. Furthermore, a correction of the HFS-based K_v by a constant offset is required but it allows a reliable R_p determination in this case study. Using a design space fed by HFS-based inputs in a MicroFD enables rapid assessment of the impact of operating parameters on product quality and process efficiency by optimization of the drying time. A drawback of the HFS-based K_v determination is the necessity to correct for a constant in the case of higher protein content. Nevertheless, future investigations should focus on quantifying the role of key variables such as the filling volume and the intra-batch homogeneity in affecting the offset between the gravimetric and the HFS-based technique, especially for lower protein content formulations. This work highlights the possibility of integrating the new HFS and MicroFD technologies in a design space application to fully implement a QbD approach whilst minimizing material usage and invested time.

CRediT authorship contribution statement

Marco Carfagna: Conceptualization, Methodology, Validation, Formal analysis, Investigation, Resources, Writing – original draft, Visualization. **Monica Rosa:** Conceptualization, Validation, Writing – review & editing, Supervision. **Andrea Hawe:** Conceptualization, Writing – review & editing, Supervision, Project administration, Funding acquisition. **Wolfgang Frieß:** Conceptualization, Writing – review & editing.

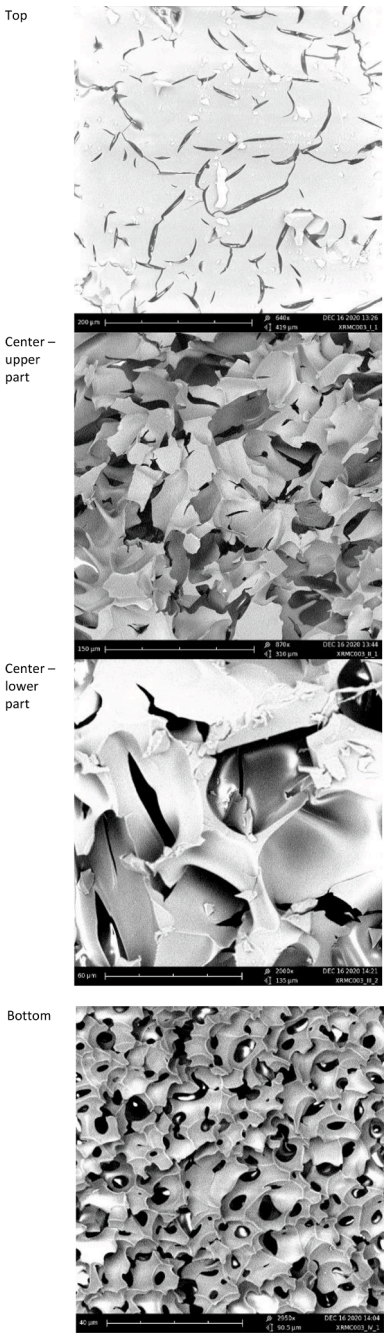

Fig. 8. Scanning electron microscopy (SEM) exemplary images from final product of the verification freeze-drying cycle.

Declaration of Competing Interest

The authors declare that they have no known competing financial interests or personal relationships that could have appeared to influence the work reported in this paper.

Data availability

Data will be made available on request.

Acknowledgement

The authors acknowledge Millrock Technology Inc. (Kingston, NY, USA) for the helpful technical support.

Funding

This research did not receive any specific grant from funding agencies in the public, commercial, or not-for-profit sectors.

Appendix A. Supplementary data

Supplementary data to this article can be found online at https://doi.org/10.1016/j.ijpharm.2023.123285.

References

Bosca, S., Barresi, A.A., Fissore, D., 2014. Use of soft sensors to monitor a pharmaceuticals freeze-drying process in vials. Pharm. Dev. Technol. 19, 148–159. https://doi.org/10.3109/10837450.2012.757786.

Butreddy, A., Dudhipala, N., Janga, K.Y., Gaddam, R.P., 2020. Lyophilization of Small-Molecule Injectables: an Industry Perspective on Formulation Development, Process Optimization, Scale-Up Challenges, and Drug Product Quality Attributes. AAPS PharmSciTech 21. https://doi.org/10.1208/s12249-020-01787-w.

Carfagna, M., Rosa, M., Lucke, M., Hawe, A., Frieß, W., 2020. Heat flux sensor to create a design space for freeze-drying development. Eur. J. Pharm. Biopharm. 153, 84–94. https://doi.org/10.1016/j.ejpb.2020.05.028.

Carfagna, M., Rosa, M., Hawe, A., Frieß, W., 2022. Design of freeze-drying cycles: The determination of heat transfer coefficient by using heat flux sensor and MicroFD. Int. J. Pharm. 621, 121763 https://doi.org/10.1016/j.ijpharm.2022.121763.

Cilurzo, F., Selmin, F., Minghetti, P., Adami, M., Bertoni, E., Lauria, S., Montanari, L., 2011. Injectability evaluation: An open issue. AAPS PharmSciTech 12, 604–609. https://doi.org/10.1208/s12249-011-9625-y.

Colandene, J.D., Maldonado, L.M., Creagh, A.T., Vrettos, J.S., Goad, K.G., Spitznagel, T. M., 2007. Lyophilization cycle development for a high-concentration monoclonal antibody formulation lacking a crystalline bulking agent. J. Pharm. Sci. 96, 1598–1608. https://doi.org/10.1002/jps20812.

Cullen, S., Walsh, E., Gervasi, V., Khamar, D., McCoy, T.R., 2022. Technical transfer and commercialisation of lyophilised biopharmaceuticals — application of lyophiliser characterisation and comparability. AAPS Open 8. https://doi.org/10.1186/s41120-022-00059-0.

Fissore, D., Pisano, R., Barresi, A.A., 2011. Advanced approach to build the design space for the primary drying of a pharmaceutical freeze-drying process. J. Pharm. Sci. 100, 4922–4933. https://doi.org/10.1002/jps.22668.

Fissore, D., Pisano, R., Barresi, A.A., 2012. Model-based framework for the analysis of failure consequences in a freeze-drying process. Ind. Eng. Chem. Res. 51, 12386–12397. https://doi.org/10.1021/ie300505n.

Tang, X., Pikal, M.J., 2004. Design of Freeze-Drying Processes for Pharmaceuticals: Practical Advice. Pharm Res 21, 191–200. https://doi.org/10.1023/B:PHAM.0000016234.73023.7.

Garidel, P., Presser, I., 2019. Lyophilization of high-concentration protein formulations. Lyophilization of Pharmaceuticals and Biologicals: New Technologies and Approaches 291–325.

Gieseler, H., Kramer, T., Pikal, M.J., 2007. Use of manometric temperature measurement (MTM) and SMART™ freeze dryer technology for development of an optimized freeze-drying cycle. J. Pharm. Sci. 96, 3402–3418.

Giordano, A., Barresi, A.A., Fissore, D., 2011. On the use of mathematical models to build the design space for the primary drying phase of a pharmaceutical lyophilization process. J. Pharm. Sci. 100, 311–324.

Goldman, J.M., Chen, X., Register, J.T., Nesarikar, V., Iyer, L., Wu, Y., Mugheirbi, N., Rowe, J., 2019. Representative Scale-Down Lyophilization Cycle Development Using a Seven-Vial Freeze-Dryer (MicroFD ®). J. Pharm. Sci. 108, 1486–1495. https://doi.org/10.1016/j.xphs.2018.11.018.

Hibler, S., Wagner, C., Gieseler, H., 2012. Vial freeze-drying, part 1: New insights into heat transfer characteristics of tubing and molded vials. J. Pharm. Sci. 101, 1189–1201. https://doi.org/10.1002/jps.23004.

Kasper, J.C., Friess, W., 2011. The freezing step in lyophilization: Physico-chemical fundamentals, freezing methods and consequences on process performance and quality attributes of biopharmaceuticals. Eur. J. Pharm. Biopharm. 78, 248–263. https://doi.org/10.1016/j.ejpb.2011.03.010.

Kauppinen, A., 2015. Raman and near-infrared spectroscopic methods for in-line monitoring of freeze-drying process. University of Eastern Finland.

Kawasaki, H., Shimanouchi, T., Kimura, Y., 2019. Recent Development of Optimization of Lyophilization Process. J. Chem. 2019 https://doi.org/10.1155/2019/9502856.

Kuu, W.Y., Obryan, K.R., Hardwick, L.M., Paul, T.W., 2011. Product mass transfer resistance directly determined during freeze-drying cycle runs using tunable diode laser absorption spectroscopy (TDLAS) and pore diffusion model. Pharm. Dev. Technol. 16, 343–357. https://doi.org/10.3109/10837451003739263.

Moino, C., Bourlés, E., Pisano, R., Scutellà, B., 2021. In-Line Monitoring of the Freeze-Drying Process by Means of Heat Flux Sensors. Ind Eng Chem Res 60, 9637–9645. https://doi.org/10.1021/acs.iecr.1c00536.

Nail, S.L., Jiang, S., Chongprasert, S., Knopp, S.A., 2002. Fundamentals of freeze-drying. Develop. Manuf. Protein Pharm. 281–360.

Narasimhan, C., MacH, H., Shameem, M., 2012. High-dose monoclonal antibodies via the subcutaneous route: Challenges and technical solutions, an industry perspective. Ther. Deliv. 3, 889–900. https://doi.org/10.4155/tde.12.68.

Pikal, M.J., Roy, M.L., Shah, S., 1984. Mass and heat transfer in vial freeze-drying of pharmaceuticals: Role of the vial. J. Pharm. Sci. 73, 1224–1237. https://doi.org/10.1002/jps.2600730910.

Pisano, R., Fissore, D., Barresi, A.A., Brayard, P., Chouvenc, P., Woinet, B., 2013. Quality by design: Optimization of a freeze-drying cycle via design space in case of heterogeneous drying behavior and influence of the freezing protocol. Pharm. Dev. Technol. 18, 280–295. https://doi.org/10.3109/10837450.2012.734512.

Sane, P., 2016. Identification and Quantification of Heterogeneity in Freezing and Primary Drying Steps of Lyophilization. Doctoral. Dissertations.

Scutellà, B., Trelea, I.C., Bourlès, E., Fonseca, F., Passot, S., 2018. Determination of the dried product resistance variability and its influence on the product temperature in pharmaceutical freeze-drying. Eur. J. Pharm. Biopharm. 128, 379–388. https://doi.org/10.1016/j.ejpb.2018.05.004.

Shire, S.J., Shahrokh, Z., Liu, J.U.N., 2004. Challenges in the Development of High Protein Concentration Formulations. J. Pharm. Sci. 93, 1390–1402.

Velardi, S.A., Barresi, A.A., 2008. Development of simplified models for the freeze-drying process and investigation of the optimal operating conditions. Chem. Eng. Res. Des. 86, 9–22. https://doi.org/10.1016/j.cherd.2007.10.007.

Vollrath, I., Friess, W., Freitag, A., Hawe, A., Winter, G., 2019. Comparison of ice fog methods and monitoring of controlled nucleation success after freeze-drying. Int. J. Pharm. 558, 18–28. https://doi.org/10.1016/j.ijpharm.2018.12.056.

Ward, K.R., Matejtschuk, P., 2019. Lyophilization of Pharmaceuticals and Biologicals: New Technologies and Approaches, Methods in Pharmacology and Toxicology. Humana Press.

Pharm Res (2021) 38:707–719
https://doi.org/10.1007/s11095-021-03023-x

RESEARCH PAPER

Micro Freeze-Dryer and Infrared-Based PAT: Novel Tools for Primary Drying Design Space Determination of Freeze-Drying Processes

Maitê Harguindeguy[1] • Davide Fissore[1]

Received: 17 November 2020 / Accepted: 23 February 2021 / Published online: 8 March 2021

ABSTRACT

Purpose Present (i) an infrared (IR)-based Process Analytical Technology (PAT) installed in a lab-scale freeze-dryer and (ii) a micro freeze-dryer (MicroFD®) as effective tools for freeze-drying design space calculation of the primary drying stage.

Methods The case studies investigated are the freeze-drying of a crystalline (5% mannitol) and of an amorphous (5% sucrose) solution processed in 6R vials. The heat (K_v) and the mass (R_p) transfer coefficients were estimated: tests at 8, 13 and 26 Pa were carried out to assess the chamber pressure effect on K_v. The design space of the primary drying stage was calculated using these parameters and a well-established model-based approach. The results obtained using the proposed tools were compared to the ones in case K_v and R_p were estimated in a lab-scale unit through gravimetric tests and a thermocouple-based method, respectively.

Results The IR-based method allows a non-gravimetric estimation of the K_v values while with the micro freeze-dryer gravimetric tests require a very small number of vials. In both cases, the obtained values of K_v and R_p, as well as the resulting design spaces, were all in very good agreement with those obtained in a lab-scale unit through the gravimetric tests (K_v) and the thermocouple-based method (R_p).

Conclusions The proposed tools can be effectively used for design space calculation in substitution of other well-spread methods. Their advantages are mainly the less laborious K_v estimation process and, as far as the MicroFD® is concerned, the possibility of saving time and formulation material when evaluating R_p.

KEY WORDS Design space · primary drying · freeze-drying process design/optimization · heat and mass transfer · mechanistic approach · model parameters

LIST OF SYMBOLS

A	parameter used to model the dependence of R_p on L_{dried}, s^{-1}.
a_{K_v}	parameter used to model the dependence of K_v on P_C, W $m^{-2}K^{-1}$
A_v	vial bottom area, m^2
B	parameter used to model the dependence of R_p on L_{dried}, m^{-1}
b_{K_v}	parameter used to model the dependence of K_v on P_C, W $m^{-2}K^{-1}Pa^{-1}$
c_{K_v}	parameter used to model the dependence of K_v on P_C, Pa^{-1}
ΔH_s	heat of sublimation, J kg^{-1}
J_q	heat flux, W m^{-2}
J_w	mass flux, kg $s^{-1}m^{-2}$
k_{frozen}	ice thermal conductivity, W $m^{-1}K^{-1}$
K_v	heat transfer coefficient, W $m^{-2}K^{-1}$
L_{dried}	dried cake thickness, m
L_{frozen}	frozen cake thickness, m
Δm	mass change, kg
$p_{w,\,c}$	water vapor partial pressure in the drying chamber, Pa
$p_{w,\,i}$	water vapor partial pressure at the sublimation interface, Pa
P_C	chamber pressure, Pa
Pi/Ba	thermal conductivity and capacitance gauges pressure ratio, −

✉ Maitê Harguindeguy
maite.harguindeguy@polito.it

[1] Dipartimento di Scienza Applicata e Tecnologia, Politecnico di Torino, Corso Duca degli Abruzzi 24, 10129 Torino, Italy

Q	heat received by the product, J
R_p	cake resistance to vapor flow, m s^{-1}
$R_{p,\ 0}$	parameter used to model the dependence of R_p on L_{dried}, m s^{-1}
T_b	product temperature at the vial bottom, K
t_d	gravimetric test duration, s
T_i	temperature at the sublimation interface, K
T_{shelf}	shelf temperature, K

INTRODUCTION

Freeze drying is a process widely used in the pharmaceutical industry to recover drug formulations from aqueous solutions. The liquid product is usually poured into vials, loaded in the freeze dryer where the process is carried out. First the solution is frozen, then the pressure is lowered, and heat is supplied to promote sublimation of the solvent (primary drying). Finally, the unfrozen water present in the product cake is removed by further increasing the temperature of the product (secondary drying) (1).

Freeze drying is a long and costly process, and is generally used over other drying methods when the drug formulation is heat sensitive (2). Notwithstanding the price, it is estimated that 16% of the top-selling 100 pharmaceuticals are freeze-dried (3). Therefore, is it imperative to have fast and efficient freeze-drying process development (and optimization) tools, shortening the time-to-market and providing benefits to the patients.

During primary drying, it is a good practice to keep product temperature below the critical temperature of the formulation, which usually is the glass transition temperature (T_g) for amorphous systems or the eutectic point (T_e) for crystalline ones. If this threshold is surpassed, changes in the cake porous structure may jeopardize product solubility, drug activity and overall product quality (4). In some cases such as nanoparticle suspensions (5), highly concentrated proteins (6) or the combined used of crystalline and amorphous bulking agents, surpassing the critical temperature may present macrocollapse, while not necessarily affecting product quality (7). Nonetheless, it is of crucial importance to identify and use the correct operating conditions that will preserve product quality.

The set of operating conditions that ensure product temperature to be below its threshold value for a given batch configuration is the design space. These operating conditions are the chamber pressure (P_C) and the shelf temperature (T_{shelf}) settings, the former defines the vapor pressure that must be achieved for sublimation to occur and the later provides the heat for sublimation. To minimize the time-to-market for a given product, it is therefore necessary to quickly identify a suitable couple of values of P_C and T_{shelf} that allow obtaining the target quality in the final product. Besides, it must be considered that primary drying alone was shown to represent 69% of the operational costs in an industrial freeze-dryer. However, the operational costs represent less than 15% of the total costs, which includes capital ones. Withal, shortening freeze-drying cycle durations increases productivity which in turn reduces the capital costs per cycle (8). To optimize the process further, the settings that maximize the sublimation rate are preferred because they make the cycle faster (9). However, solvent flow rate must be compatible with the freeze-dryer condenser capacity and also with the features of the duct connecting the chamber to the condenser, to avoid choked flow (10–12). Thus, these optimal settings must be carefully selected within the design space.

To obtain the design space, empirical and mechanistic approaches can be used. An empirical approach can be performed by a non-expert practitioner, but it requires many time-consuming experiments to determine the relationship between the operating conditions and the resulting process. Besides, this approach is only valid in situ, which limits the scalability of the results found at lab-scale, where these experiments may be carried out (13, 14). Mechanistic approaches, on the other hand, allow mathematical modelling of the product temperature, water vapor flow and drying time throughout a process as a function of the chamber pressure and shelf temperature (15–18). Such models are based on heat and mass transfer balances and can be used once parameters like the global heat transfer coefficient (K_v) and the cake resistance to vapor flow (R_p) are known. When this approach is used, fewer experiments are needed with respect to the empirical approach to obtain a comprehensive design space for a product. Nonetheless, even when using a mechanistic approach, the design space determination for a formulation is a time-consuming task.

The gravimetric method (15, 19, 20) is regarded as the standard method to obtain K_v; however, many alternative methods have been proposed. In general terms, if reliable product temperature monitoring and primary drying endpoint determination tools are in place, non-gravimetric K_v estimations can be obtained. Many of the alternative methods are based on the pressure rise test (PRT) using different algorithms, varying in complexity. Some of this methods are the Pressure Rise Analysis (PRA) (21), the Manometric Temperature Measurement (MTM) (22), Dynamic Parameters Estimation Method (DPE) (2) and its more straightforward version DPE+ (23). Other methods presented were based on a heat flux sensor (24) and Tuneable Diode Laser Absorption Spectroscopy (TDLAS) (25–27) to cite a few. Some advantages can be obtained with these methods, for instance, the determination of K_v at different pressures in the same run using a heat-flux sensor. The main drawback is that a mean value of K_v is obtained for the batch, without differentiating between the central vials, heated just through the shelf, and the edge vials, heated also through other

mechanisms, e.g. radiation from chamber walls and door (19), while gravimetric test provides a very detailed picture of the system. As far as R_p is concerned, it may be estimated as well as by means of PRT-based algorithms (23, 28), through TDLAS (29), or using the product temperature measurement in a run (30).

In this study, we present two methods for design space determination, based on the following devices:

i. An Infrared (IR) process analytical technology (PAT) tool for monitoring a lab-scale freeze-dryer to obtain R_p and a non-gravimetric K_v estimation in a non-invasive way, i.e., without using thermocouples (to the authors' knowledge, this is the first time this has been successfully implemented using this type of sensor).
ii. A micro freeze-dryer, to obtain the model parameters R_p and K_v using fewer vials than usual.

As a base for comparison, the standardly used tool for mechanistic approaches, a freeze-dryer equipped with thermocouples, is also presented. The model parameters and design spaces obtained through the innovative methods are compared to the ones obtained using the standard methods for verification of their applicability. The design spaces for central batch conditions for two different systems, an amorphous and a crystalline one, are tested. Central batch conditions are those applicable to central vials in a batch, i.e., those with at least 6 neighbouring vials. Central vials typically correspond to more than 90% of the vials in industrial batch processes. Thus, the design spaces for edge vials, those with 5 of less neighbouring vials, are not presented in this study. The advantages and limitations of each novel approach are also discussed throughout this study.

MATERIALS & METHODS

Equipment

The experiments were carried out in two freeze dryers, a lab-scale one (REVO®) and a small scale one (MicroFD®), both produced by Millrock Technology Inc. (Kingston, NY, USA). The shelf temperature can be set from −70°C to +65°C in the REVO® and from −60°C to +60°C in the MicroFD® freeze-dryer. The REVO® has roughly 1 m^2 of total shelf area and it is provided with an external condenser with maximum condensing capacity of 30 L operated at approximately −80°C. The MicroFD® has a chamber with a 15-cm-diameter circular shelf where the vials are loaded, encircled by removable thermal conductors. These conductors ensure the contact between the external vials of the batch and the temperature-controlled aluminium ring (LyoSim®). The LyoSim® is used to emulate the desired heating conditions observed in a larger batch, whether for edge or central batch conditions. To this end, the ring temperature can be set to range from −15°C to +15°C offset with respect to the average product temperature.

Chamber pressure was monitored in both freeze-dryers using a thermal conductivity (Pirani type) and a capacitive (Baratron type) pressure gauge. The ratio between these two pressure signals (*Pi/Ba*) was used to estimate the duration of the primary drying stage. The pressure profile by the Pirani gauge exhibits a sharp decreasing trend as the drying process comes to an end. The start of this inflection is defined as the onset time while the end of it is defined as the offset time (4). The time interval between these two points can be used to infer batch heterogeneity, while the drying duration lays, typically, between them. This is a broadly used method, while the use of the offset point to determine the end point is a good practice to ensure drying of all vials (31, 32). Both systems were equipped with T-type thermocouples (Tersid, Milano, Italy) for temperature monitoring. Additionally, an infrared sensor was used to monitor product temperature, when applicable.

The IR sensor used in this study (IMC Service S.r.l., Italy) is the same sensor presented by Harguindeguy & Fissore (33) to monitor batches also using the REVO® freeze-dryer. This system has a built-in thermal camera (FLIR Systems model A35; FLIR Systems Inc., Wilsonville, OR, USA), a processing board, and a Wi-Fi antenna for wireless data transfer. The IR sensor was placed inside the chamber, 25 cm away from the vials being monitored and on the same shelf. It was aligned with the shelf centreline, against the rear of the chamber. Placing the sensor in this way allows monitoring the whole cake axial profile, from the cake bottom to the top. The sublimation interface temperature is measured and tracked as the minimum axial temperature. The bottom temperature is the average temperature at the bottom acquisition pixels, both computed as previously described (33).

Model Parameters

One-dimensional models, assuming negligible temperature and composition gradients in the radial direction of the vial, are able to well represent product temperature dynamics (34). They assume that the heat flux to the product is proportional to the temperature difference between the shelf temperature and the temperature of the product at the bottom of the vial (T_b):

$$\dot{J}_q = K_v\left(T_{shelf} - T_b\right). \quad (1)$$

The water vapor mass flux from the sublimation interface to the drying chamber is proportional to the difference between their water vapour partial pressures, where the chamber water partial pressure can be assumed to be equal to

the chamber pressure (P_c) as the gas in the chamber is about 100% water vapor:

$$J_w = \frac{1}{R_p}\left(p_{w,i} - p_{w,c}\right), \tag{2}$$

$p_{w,\,i}$ may be calculated by Eq. 3, where T_i can be approximated to T_b when the cake height and R_p are low. In the present study these differences were smaller than 1°C during primary drying, as experimentally measured by the IR sensor.

$$p_{w,i} = e^{\left(28.935 - \frac{6150}{T_i}\right)}. \tag{3}$$

The one-dimensional model used here is based on the energy balance at the sublimation interface (34):

$$J_q = \Delta H_s J_w, \tag{4}$$

stating that all the heat arriving to the interface of sublimation is used for ice sublimation. This equation (Eq. 4) may be used once K_v and R_p are known. With respect to the overall heat transfer coefficient K_v, a gravimetric test may be carried out as described by many in the literature (16, 24, 35). In such tests, the total heat received by the vials (Q) is assumed to be used for water sublimation, quantified by the weight loss (Δm) in each vial after a truncated sublimation cycle:

$$Q = \Delta m \Delta H_s. \tag{5}$$

The amount of heat received by the product can be also expressed as:

$$Q = K_v A_v \int_0^{t_d} \left(T_{shelf} - T_b\right) dt, \tag{6}$$

where t_d is the duration of the sublimation step of the gravimetric test and A_v is the cross-section area of the vial. With Eq. 5 and Eq. 6, it is possible to determine K_v if T_{shelf} and T_b are known. The global heat exchange coefficient, K_v, may be also obtained at the end of a full primary drying cycle given that also the drying end-time is accurately determined. In fact, at the end of the drying process, Δm corresponds to the initial amount of water in each vial, and Eq. 6 may be used to get K_v by setting t_d equal to the duration of the primary drying stage.

The heat exchange coefficient depends mainly on the type of vial used and on the chamber pressure, whereas the heating fluid temperature has a negligible effect (19). This way, K_v can be estimated as a function of pressure for a given product-vial set up (36) as illustrated in Eq. 7:

$$K_v = a_{K_v} + \frac{b_{K_v} P_c}{1 + c_{K_v} P_c}. \tag{7}$$

The K_v fit coefficients b_{Kv}, c_{Kv} give the dependence of K_v on P_c and their dependence on the equipment can be neglected. The coefficient a_{Kv}, on the other hand, has a high dependence on the equipment and on the position of the vial over the shelf (37).

To obtain R_p, first the K_v for that batch configuration and settings must be known. Then, product temperature must be monitored for the studied formulation during a drying cycle (where the operating conditions are set in such a way that cake collapse is avoided). Using Eq. 1 J_q is obtained to then obtain J_w through Eq. 4. Since $p_{w,\,i}$ is a function of product temperature and $p_{w,\,c}$ can be assumed to be equal to P_c, R_p can be obtained using Eq. 2.

R_p can be described in function of the dried cake thickness (L_{dried}), which can be calculated based on the water mass flux (J_w) (28). To account for this dependence between R_p and L_{dried}, Eq. 8 is frequently used (36, 38, 39).

$$R_p = R_{p,0} + \frac{AL_{dried}}{1 + BL_{dried}}. \tag{8}$$

In this model, $R_{p,\,0}$, A and B are fitted experimentally based on the R_p vs. L_{dried} values.

To simulate in silico the process as it progresses and calculate T_b according to how much frozen cake is still left, Eq. 9, i.e., the steady-state heat balance for the frozen product, can be used:

$$T_b = T_{shelf} - \frac{1}{K_v}\left(\frac{1}{K_v} + \frac{L_{frozen}}{k_{frozen}}\right)^{-1}\left(T_{shelf} - T_i\right). \tag{9}$$

The sublimation interface temperature, T_i, is calculated recursively together with $p_{w,\,i}$ and R_p, using Eq. 2–4 and Eq. 8–9 for each integration interval. Twenty-second intervals were used in this simulation. Once T_i is found, T_b can be calculated for any stage of freeze drying, i.e., for any given percentage of frozen cake left. In Eq. 9, k_{frozen} is the ice conductivity. The k_{frozen} value used was, 2.55 W/mK (40), corresponding to the ice conductivity at −35°C.

Design Space

For design space estimation using a mechanistic approach, the model parameter K_v must first be determined as a function of chamber pressure, as presented in Eq. 7. To this end, at least three gravimetric tests should be carried out at different pressures as described in Fissore et al (36). These gravimetric tests can be performed with water to save formulation material and preparation time as the solution composition has no effect on the resulting K_v (15).

For R_p estimation, at least one complete primary drying cycle should be performed for the target formulation. It is important to ensure that product temperature during this test is kept below the threshold value for that product. Otherwise, cake collapse takes place, leading to misestimation of the R_p profile. If this happens, product temperature during primary drying will be also misestimated and

the resulting design space will not ensure product quality (14).

Having these parameters properly computed, the T_{shelf} and P_c combinations that will ensure product T_b to be below the formulation threshold value can be calculated. Eq. 1–4 can be used to this end, determining the possible T_{shelf} and P_c combinations for each and any point of primary drying progress, defined by the residual L_{frozen}. This way, for each pressure value being considered in the design space, the product T_b for the regarded L_{frozen} is calculated by testing different T_{shelf} values. Thus, the T_{shelf} values that ensure product T_b to be below its threshold limit comprise the design space for that pressure and considered L_{frozen} value. The threshold limit, i.e., the maximum allowed temperature for the case-study formulation is usually the T_g or T_e. Additionally, once the T_{shelf} and resulting T_b values for each pressure are known, J_w for any desired L_{frozen} can be calculated for the whole design space. This can be used to further optimize the process duration, by choosing the conditions within the design space that will maximize the sublimation flux.

It is important to point out that, since R_p has a dependence in L_{dried} the predicted T_b values for different T_{shelf} and P_c combinations will also vary according to the L_{dried} portion considered. Since R_p reaches its maximum value towards the end of drying, so does T_b. Fissore et al (36) proposed the estimation of a design space including the L_{dried} as a third coordinate to account for this dynamic behaviour. In this study, we consider a static environment, i.e., one single T_{shelf} to be used throughout primary drying. To this end, all calculations are based on a critical T_b value using as a reference the moment when only 10% of frozen cake remains.

The use of a dynamic parameter estimation algorithm (38), manometric temperature measurement (41) and the use of a combined statistical and mechanistic approach (42) were proposed for design space estimation. However, the use of a pilot-scale or lab-scale freeze-dryer using thermocouples to monitor product temperature is still the most common tool used for the mechanistic approach. Typically, three gravimetric tests are performed for K_v estimation and one for R_p, as decribed above. However, such experiments can be time consuming which increases operational costs. Specially the vial-weighting steps required for the gravimetric tests are laborious, considering that such batches usually have a few hundred vials. Additionally, poor thermocouple placement many times compromises batch monitoring if a non-expert performs this task (43).

Reference Method

Design space estimations for central vial conditions using a lab scale freeze dryer (REVO®) were done. Each batch had 210 vials disposed in a hexagonal array (14 rows with 15 vials each, 156 central vials). Six thermocouples were placed in central vials for temperature monitoring. Figure 1 illustrates the batch configurations used for each of the tested methods.

IR-Based PAT Method

The use of an infrared sensor to monitor batches with up to 157 vials in the REVO® freeze-dryer was verified previously (33). Inspired by a previous study (44) on the measurement of thermal profiles in vials in different batch positions, an extrapolation was done. This aimed to address the IR sensor main limitation (33) when monitoring freeze-drying batches, i.e., its field of view. In that study (44), first row vials in a more shielded position in the hexagonal array configuration were shown to present a closer behaviour to central vials, although they are still different. The use of a hexagonal array permitted better batch representativeness in IR-monitored batches (33). The first row vials, in the rear of the chamber, that were slightly shielded by their side vials in this array configuration, were regarded as representative of central vials. They have only five neighbouring vials, instead of six, as a common definition of central vials. Nonetheless, this approximation allowed the estimation of model parameters, K_v and R_p, for central batch conditions with good accuracy. Additionally, through monitoring of the sublimation interface temperature (T_i) throughout primary drying, a consistent determination of the endpoint was achieved (33). The primary drying duration was determined in the same way presented by Harguindeguy & Fissore (33). The same custom MATLAB (MATLAB R2019b © 1994–2020 The MathWorks, Inc) code was used. First, a curve was fitted to the T_i data to allow the use of the first derivative to infer the inflection points in an automated way. The inflection point of interest is the ascending interval observed when sublimation is completed, and the heat supplied by the shelf is used as sensible heat. Since the IR sensor is non-invasive, the detection of this rising profile is much more accurate than the one observed using thermocouples and can be used to correctly infer the end of sublimation. The fitting used was a non-parametric smoothing spline, which fits a set of intersecting polynomials to the data. The function is controlled by a smoothing parameter which, the higher it is, it makes the fit smoother. The fit was calculated using MATLAB built-in *smoothingspline* function with the default parameter set (45).

Based on these findings (33), by monitoring three complete cycles using the desired formulation, the whole design space can be obtained without performing gravimetric tests. The K_v and R_p values are obtained based on the T_i profiles of these vials, regarded as representative of central batch ones. Eq. 5 and Eq. 6 can be used to calculate K_v, assuming complete sublimation of the water present in the monitored vial and determining the primary drying duration by the T_i infrared-based method. R_p is directly obtained based on the T_i profiles of the monitored vials as previously discussed.

For these tests, 105 vials were used (14 rows with 7 or 8 vials each, 66 central vials) since some space is required to place the infrared sensor inside the chamber. Using the same equipment and settings, no significant differences were reported for the K_v values between these smaller IR-monitored batches and large thermocouple-monitored ones. Moreover, the effect of this sensor inside the chamber was found negligible while the shelves' configuration was kept the same across all tests (33). Since the front row has 14 vials, this estimation is based on the profiles of the 6 more shielded vials in this row. This low number of samples could be a limitation to this method. However, the results for all tested conditions were satisfactory as reported ahead.

MicroFD® Method

The use of the MicroFD® with a LyoSim® offset temperature of −5°C with respect to the product temperature resulted in good batch homogeneity (46). Moreover, this offset setting was found to be a good emulator of central batch conditions in the REVO® freeze-dryer (35). This −5°C setting was also found to represent well the temperature profiles and K_v values of central batch vials in another freeze-drying equipment of similar scale, the LyoStar® III lyophilizer (SP Scientific, Warminster, PA, USA) (30). To determine the design space using a micro freeze-dryer, the traditional three gravimetric tests (for K_v estimation) and a complete primary drying cycle (for R_p estimation) should be performed. However, since the batch has a very small number of vials (19 in this case), the task becomes much easier, less time consuming and requires less formulation material than the usual. The MicroFD® may also be equipped with a heat flux sensor, AccuFlux®, allowing for a direct measurement of the heat flux to the product in the vials: this allows avoiding weighing the vials before and after the gravimetric test, thus further simplifying the experiments. This tool, however, was not used in the present study to reduce the degree of freedom between the methods being compared. Thus, K_v was estimated gravimetrically and R_p based on Eqs. 1 and 2.

Products and Vials

To determine the design space for amorphous and crystalline systems, tests were carried out using 5% sucrose and 5% mannitol aqueous solutions. Both sugars were purchased from Sigma Aldrich (≥99.5%) and used as received. Solutions were processed in 6R tubing vials (Schott Pharmaceutical Packaging, Inc., Lebanon, PA, USA) using a 3 mL fill volume, resulting in a 11 mm cake height.

All vials were placed directly onto the shelf and were partially stoppered using an igloo stopper (NovaPure Chlorobutyl Igloo Stoppers, West Pharma, Exton, PA, USA) after filling. Vials monitored using thermocouples had holders (VTH-M-0020, Millrock Technology Inc. Kingston, NY, USA) that enabled careful control and correct placement of the thermocouples used, touching the bottom of the vial (46).

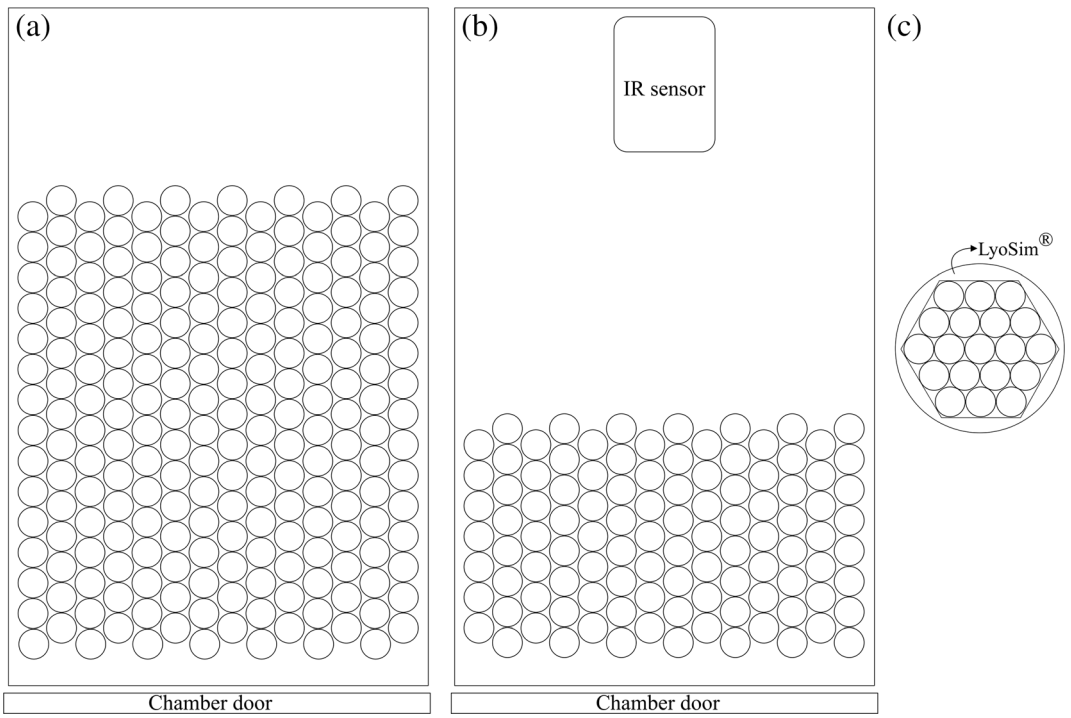

Fig. 1 Representation of the set ups used, as seen from above, for: (**a**) the reference method, (**b**) the IR-based method (both in the REVO® freeze dryer), and (**c**) the MicroFD® method.

Design of Experiments

For all methods, the K_v estimation as a function of pressure was done at 8, 13 and 26 Pa. The R_p profile for sucrose solution was obtained using a − 20°C shelf temperature and 8 Pa chamber pressure setting, while for mannitol it was obtained using 0°C and 13 Pa.

The definition of the threshold temperature depends on the formulation system as mentioned, but it also depends on the tolerable final product quality. For sucrose 5%, Horn and Friess (47) reported a T_g of −33.7°C (7). If small micro collapses are allowed, however, a maximum product temperature value of up to −32°C could be accepted (37). In this study, the threshold temperature for sucrose was defined as −33°C.

Mannitol formulations usually have a more stable cake structure, resulting in elegant final products with no observable shrinkage. Still, mannitol systems may present different polymorphs together with an amorphous phase (48). A 10% crystalline mannitol formulation presenting α-mannitol and β-mannitol polymorphs, with the former as the most abundant one, was found to have a melting temperature of −21.5°C (49). For pure amorphous mannitol, i.e., not in solution, a 13°C collapse temperature for was reported (48). Through differential scanning calorimetry (DSC) analysis, a 10% amorphous mannitol formulation was found to have two T_g points, one at −35°C and one −25°C (50). This formulation also showed a subsequent crystallization exotherm peak, showing the strong tendency of mannitol towards crystallization which makes it a stable cake forming agent (50, 51). Melting for this formulation was observed near 0°C, which was attributed to ice melting. Since lyophilization is based on operating below the water triple point, this melting transition should not affect freeze-dried formulations. Still, lyophilization is generally used for heat sensitive molecules, for this reason a threshold value of −15°C was chosen for the design space calculation of the 5% mannitol solution.

Statistical Analysis

Statistical analysis was used only to compare the K_v values obtained through the proposed tools with the reference approach (gravimetric tests in the REVO® freeze-dryer, using thermocouple measurements). The evaluations done always compared the group values in pairs. For example, the K_v values at 13 Pa obtained in the micro freeze-dryer versus the ones obtained in the REVO® at the same pressure. This way, first, a normality test was performed on each group of results and then they were compared using a Student's t test (52). The t-tests done were two tailed, two-sample (independent) t-tests assuming an unknown variance. A 99% confidence interval was used for both the normality tests and the t-tests.

RESULTS

Model Parameters for Design Space Calculation

To evaluate the applicability of the proposed tools for design space estimation, first, their ability to properly obtain the model parameters must be verified. These critical model parameters are the K_v values at different pressures and R_p values for each of the tested solutions. If the values found using the proposed devices are comparable to the ones obtained through the reference method, so should be the resulting design spaces.

The average K_v values found in each system under the tested pressures were all comparable, as illustrated in Fig. 2. Compared to the reference method, the biggest differences were observed when using the IR-based method. These differences were of 6.3%, 8.4% and 8.1% for 8, 13 and 26 Pa, respectively. For the micro freeze-dryer, these differences were very low for 13 and 26 Pa, representing a 1.3% and 2.4% difference, respectively. For 8 Pa however, it reached a 6.5% difference against the reference method. Nonetheless, through statistical analysis via t-tests, the global heat exchange coefficients found using the MicroFD® and the IR-based method were not statistically different from the values obtained in the REVO® freeze-dryer using the gravimetric test ($p > 0.01$).

Once the K_v determination obtained through the proposed tools was deemed equivalent to the values found by the reference method, the accuracy in R_p determination for each tested formulation by the novel tools was examined. As investigated by Scutellà et al. (28), the cake resistance to vapor flow affects product temperature during drying. The whole purpose of

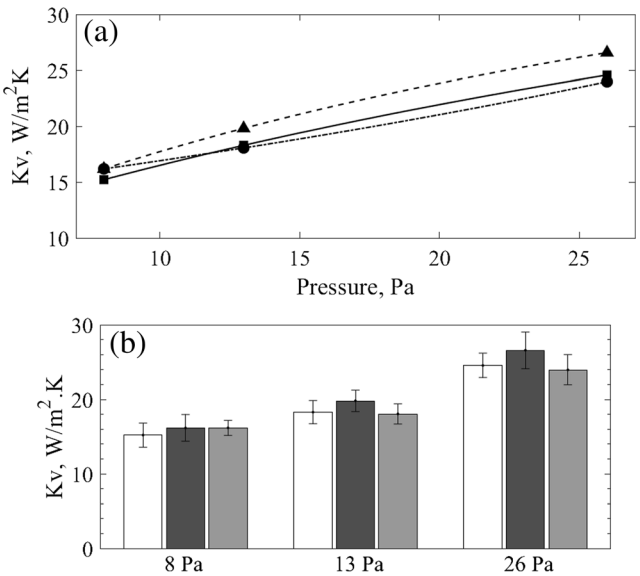

Fig. 2 (**a**) K_v values with curve fit using Eq. 7 for the standard method (−■), the IR-based method (–▲) and the MicroFD® (−.●). (**b**) Bar chart for K_v values for the standard method (white), the IR-based method (dark grey) and the MicroFD® (light grey). Error bars indicate one standard deviation.

calculating the design space is to ensure product temperature stays below its threshold value. Thus, correct R_p determination is of crucial importance. Since the R_p calculation is based on product temperature, the resulting profiles using the different proposed tools will be similar if the product temperature profiles are also similar. One of the most important aspects of the observed R_p profiles is the maximum value it reaches. This maximum will also dictate when the maximum product temperature will be observed, thus representing a critical control point for a given formulation.

Figure 3 presents the R_p results found for each solution. As it can be seen, for all tested tools the R_p profiles seem comparable, i.e., they are within the same order of magnitude and the values are quite correspondent. The temperature profiles measured by thermocouples towards the end of primary drying are not reliable because there may be a loss in contact between the sensing element and the surrounding ice (31). Moreover, unless the process is conducted by a well-trained operator, thermocouple misplacements are done, resulting in inaccurate temperature measurements (11). Additionally, even when a trained operator places the thermocouples properly, they may move during the loading process or the cake may break in such a way that it is not anymore representative of the process. Essentially, the main issue is the lack of consistency between thermocouple measurements. Many times, vials subjected to virtually the same batch conditions, present varying rising temperature profile times (31). IR thermography offers a solution to this issue since it is a non-invasive sensor and experimentally, the rising of the temperature profiles is more consistent across different vials. However, it has its own limitations as well. The IR sensor monitors the product within its field of view, which is the external product layer, in contact with the vial wall. The temperature profiles measured by the IR camera represent well the external cake layer, but they do not represent very well the last, lower inner core of the frozen product. This way, the raw R_p profiles observed in Fig. 3 rise before the completion of sublimation for all tested tools. That is why the fitted curves (Eq. 7) are very handy in process calculations to estimate the effective R_p profiles and resulting product temperatures during a process.

The durations of the process using each tested method do not directly impact the design space calculation but can also give a good clue regarding the equivalence between the tested systems. If the global heat exchange coefficient and cake resistance to vapor flow are similar between systems, so should be the overall process duration. As seen in Table I, based on the *Pi/Ba* curve onset and offset points, the primary drying durations were all comparable. The onset time represents the point in which drying is complete for many vials in the batch, but not yet for all of them. By the offset point, drying is complete in all vials in a batch. It is important to compare the onset and offset times together due to the large variability intrinsic to this method. These points vary according to batch size, drying conditions and equipment characteristics (31). Thus, of course they are not the *same* as the chamber volume and vacuum pump are different between the REVO® and MicroFD®. Additionally, when the IR sensor was used, the batch size, and consequently the total solvent volume, was half the size of the full REVO® batch. The time difference between the onset and offset signals derives from the batch heterogeneity, but also increases with batch size. Additionally, the *Pi/Ba* signal was found to start decreasing when the sublimation rate becomes smaller than a threshold value of 2×10^{-6} kg.s^{-1}, which may vary according to the equipment and its design (31). Thus, considering the intrinsic variability of the *Pi/Ba* onset and offset signals, the primary drying durations observed using all tested methods may be considered to be in good agreement.

Calculation of the Design Space

The design space calculation depends heavily on the K_v and R_p values found for a given product, vials used and batch configuration. Since these parameters presented a good equivalence across the systems, a similar behaviour is expected for the resulting design spaces. Figure 4 presents the upper limit of shelf temperature and chamber pressure settings for the last 10%

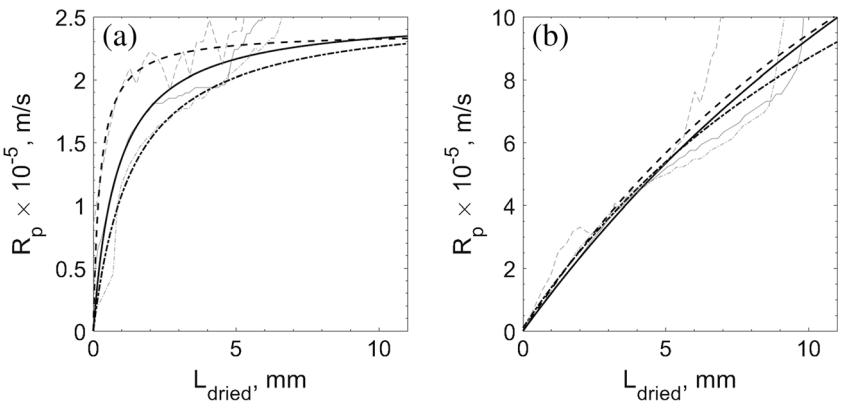

Fig. 3 R_p profiles for (**a**) 5% sucrose using 8 Pa and − 20°C shelf temperature and for (**b**) mannitol 5% sucrose using 13 Pa and 0°C shelf temperature. The raw data are plotted in light grey colour while the fitted curves for the standard method (−), the IR-based method (–) and MicroFD® (-.) are in black.

Table I Primary Drying Estimated Durations in Hours Based on the *Pi/Ba* Onset and Offset Points

	Sucrose 5%		Mannitol 5%	
	Pi/Ba onset	*Pi/Ba* offset	*Pi/Ba* onset	*Pi/Ba* offset
MicroFD®	24.7	29.2	15.3	19.1
REVO-IR	25.6	33.1	15.0	16.8
REVO	28.2	33.2	16.9	20.1

of frozen cake obtained through all the tested methods. As it can be seen, the resulting design spaces for sucrose are practically *the same* whether they were calculated based on the proposed tools or the reference method. For mannitol, some small differences were observed in the design spaces. In the case of the MicroFD®, the lower R_p profile for mannitol compared to the reference method resulted in slightly higher usable T_{shelf} settings, which was more evident for higher pressures, where the MicroFD® K_v was smaller than the reference one.

Simulating in silico the freeze-drying process until the last 10% of cake, as described in materials & methods, the product bottom temperatures (T_b) were calculated. With this T_b and Eqs. 1 and 4, $\mathcal{J}_w$ curves for different T_{shelf} and P_c values (since it will change the K_v) were calculated. This information coupled with the design space allows further optimization towards reducing the required primary drying time when higher sublimation rates are chosen.

As presented in Fig. 5, the direction towards higher sublimation rates for sucrose is along the lower pressures, which is in accordance with previously reported results (18, 36, 37). When lower pressures are used, K_v also decreases allowing higher shelf temperatures. This increased shelf temperature setting provides more heat for sublimation without compromising the cake structure. According to these results, the optimal direction for choosing the operating conditions is towards the left and the top. However, in Fig. 6, the sublimation flux curve behaviour was different, more convex, making optimization direction to be towards higher pressures. This means that the increase in K_v when operating at higher pressures contributes more to the sublimation rate than the decrease in vapor pressure when operating at low chamber pressure settings. At first glance, this may seem different from previously reported sublimation flux contour plots (18, 36, 37); however, it is not quite the case. Taking a closer look on some previously published $\mathcal{J}_w$ contour plots (18, 36, 37), it is clear that the curves have a concave profile at lower T_{shelf} values which increasingly becomes less concave with higher T_{shelf} values, until it finally becomes convex. This matter did not affect the optimization direction of those design spaces because the change in the profile profile only occurred around the T_{shelf} upper limit. The same can be observed on Fig. 5. However, for mannitol, the T_{shelf} upper limit in Fig. 6 is roughly 15°C higher than previously calculated (18) due to the higher threshold temperature chosen in this present study. This explains the apparent differences observed in the $\mathcal{J}_w$ contour plots, having a convex profile.

It is important, however, to remember that the design spaces presented here are built for central batch conditions. Since edge vials would heat up more due to less shielding, in this case it is advisable to operate within a safety margin. In fact, it is always advisable to operate under a safety margin to ensure product quality (53). For central batch conditions, a safety margin of 2°C was proposed, considering only the variability in vial dimensions, which affects the vial K_v. Moreover, the authors suggested that the safety margin for vials subjected to edge effects could be in the same order of magnitude of the 2°C reported value (16). Another alternative is to use the proposed tools to determine the design space considering edge vials. The proposed tools in this study can be used to determine the design space based on edge vials simply by changing the settings used for K_v determination. However, choosing operating conditions aiming to preserve product quality in edge vials is not practical in industrial applications. In such cases, batches are very large and edge vials comprise a small percentage of the whole batch. Since edge vials receive much more heating from the chamber walls than central vials, substantially lower shelf temperatures should be used. As seen from the $\mathcal{J}_w$ results, this would increase greatly the total required drying time, representing a big increase in processing costs just to preserve a very small percentage of the batch. Longer cycles with lower shelf temperatures

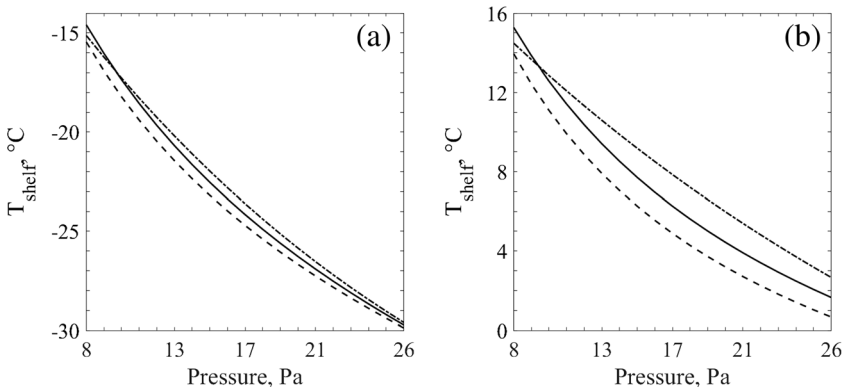

Fig. 4 Design spaces for the last 10% of frozen cake obtained through the novel tools compared with the one obtained through the standard method. Lines plotted for the standard method (−), the IR-based method (–) and the MicroFD® (−.). (**a**) Results for sucrose 5% and (**b**) for mannitol 5%.

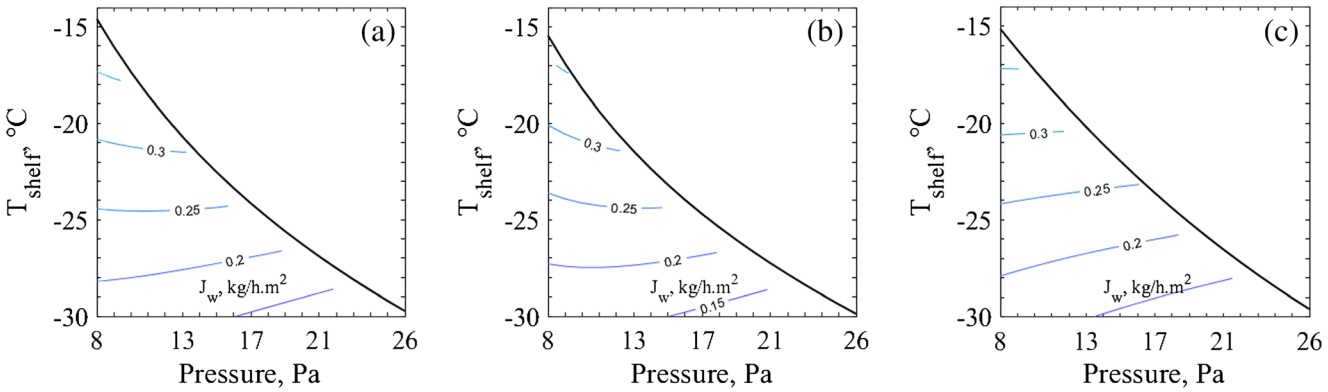

Fig. 5 Design space for 5% sucrose considering coupled with the respective J_w contour plots. Obtained through (**a**) the MicroFD® (**b**) the IR-based method and (**c**) the standard method.

can ensure product quality for the whole batch, but also mean less batches produced per year, which increases the capital costs per cycle. The final decision on how to design a cycle will be based on what delivers a quality product at the fairest price to the patients.

Comparing the behaviours of the T_{shelf} and P_c upper limit line together with the $\tilde{J}_w$, it can be appreciated that the MicroFD® tended to have a more linear behaviour than the observed ones for the IR-based method and the reference approach (both in the REVO). This is simply a direct reflection of the behaviour of the fitted curve to K_v, also more linear and it does not have any relevant physical meaning. In fact, the variation between the resulting design spaces using the novel tools in comparison to the reference method is irrelevant from the practical point of view, because it is advisable to operate with a safety margin as above-mentioned.

Final Considerations on the Design Spaces Obtained

To verify the applicability of the obtained design spaces, product temperature must stay below the threshold value when operating under these conditions for a REVO® full batch, with 210 vials. Considering all previous similarities in K_v and R_p between the different methods, this is expected to happen. As follows, Fig. 7 shows the temperature profiles and pressure ratios (Pi/Ba) observed through a complete primary drying cycle for both tested solutions. The tests presented were the same ones used to determine the R_p profiles for the reference method. For both products, the conditions chosen are below the T_{shelf} and P_c pairs upper limit by a margin and, so do the resulting temperature profiles.

As it can be observed, product temperature was kept well below the defined threshold values. As explained above, thermocouple measurements are not reliable towards the end of primary drying. Thus, if by the end of primary, the temperature profiles are above the threshold value, that may not represent product jeopardy. In freeze drying, as in many other processes, several factors influence the final product quality, this way, a holistic analysis of the results is preferred over a reductionist one, which relies on just one sensor or attribute to evaluate and develop a cycle.

DISCUSSION

The heat and mass transfer coefficient results are in accordance with previous findings. The same IR sensor was previously applied to the same batch configuration of 6R vials using

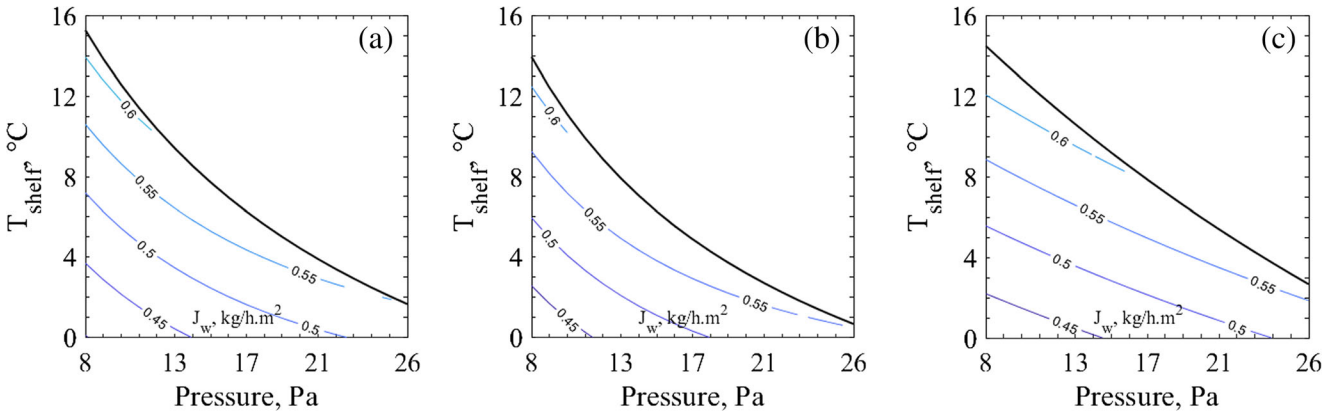

Fig. 6 Design space for 5% mannitol considering coupled with the respective J_w contour plots. Obtained through (**a**) the MicroFD® (**b**) the IR-based method and (**c**) the standard method.

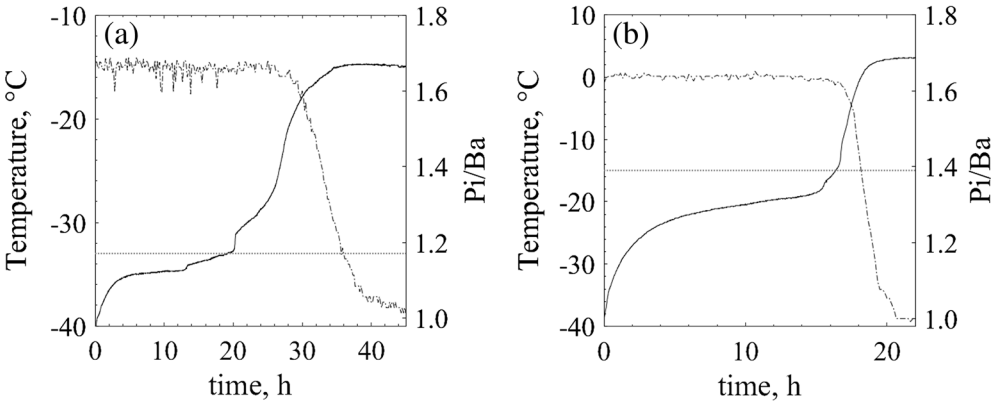

Fig. 7 Product temperature (—) and pressure ratio signal (—.) during primary drying for the standard method (REVO® full batch monitored through thermocouples) using (**a**) sucrose 5% at −20° and 8 Pa. (**b**) mannitol 5% at 0°C and 13 Pa. The horizontal (..) grey lines show the threshold temperature for each solution.

8 Pa and − 20°C as operating conditions. In that experiment, K_v was calculated gravimetrically using the temperature profile provided by the infrared sensor. The resulting K_v found in that study was 16.7 ± 2.3 W/m^{2}K (33). In this present study, the non-gravimetric K_v estimation resulted in 16.2 ± 1.8 W/m^{2}K. For the MicroFD®, using the −5°C offset setting for the LyoSim®, K_v values in the MicroFD® were found correspondent to REVO® central batch ones (35). The observed R_p values found in this study were also in good agreement with previously reported values (18, 28).

It can be appreciated that the resulting design spaces obtained through the different tested tools and approaches are all in good agreement. It is important to remember, however, that these results consider a static design space. Thus, only one shelf temperature setting was used, considering the last 10% of frozen cake as a critical control point in this process. Still, the design space is a result of the process parameters K_v and R_p. Since there was a good equivalence between the proposed tools and the reference method, the results suggest these tools could be also used considering different percentages of remaining frozen cake. This would allow the development of a dynamic design space, taking advantage of the lower $R_p$values in the beginning of drying to use higher T_{shelf} values and decrease the required drying time.

Furthermore, to scale the design space obtained using the reference method up to an industrial freeze dryer, only one extra gravimetric test may be sufficient as described in Fissore et al. (18). One test is enough in fact to determine the a_{Kv} coefficient from Eq. 7, the only one with a relevant dependence on the equipment, given that the fit was already done in a lab-scale or pilot-scale freeze dryer. The R_p should also be obtained for the industrial equipment, but again just one test would be enough for a given formulation. This scale-up method can also be analogously used for the proposed novel tools, since such a good agreement was found between the tested methods. Regarding chocked flow, in lab scale this is typically less usual due to the equipment design (18). Still, it can be an issue when high sublimation rates are used for industrial scale freeze-dryers. To address this, the industrial equipment should be tested at full capacity and different pressures as described in Patel et al. (12). This should be done just once and it can be used for all future process design for that piece of equipment.

CONCLUSIONS

Both alternative methods investigated in this paper for design space estimation present advantages and limitations. The non-gravimetric K_v determination obtained using the IR camera is favourable in terms of not having to weigh numerous vials before and after primary drying. Additionally, with just a complete run K_v and R_p profiles can be promptly obtained. However, it is time consuming since the entire drying cycle must be performed at each tested pressure. Is it important to point out, as mentioned in the introduction, that there are other methods which allow a non-gravimetric estimation of K_v and the estimation of R_p. Many are based on the Pressure Rise Test; some rely on Tuneable Diode Laser Absorption Spectroscopy or use a heat flux sensor, for instance. These methods also present advantages of making K_v and R_p determination less laborious. Still, another issue to be taken into consideration for the IR-based method is the cost as each run requires the use of the actual product. This way, this method is recommended mostly when the tested product is not prohibitively expensive, and when the time required to prepare the batch, to load/unload the vials and to defrost the condenser is not a concern.

The MicroFD® once again showed its practicality and applicability. K_v can be estimated by the traditional method, i.e., gravimetrically without much hassle since only 19 6R vials are needed. The MicroFD® is equipped with a heat-flux sensor, AccuFlux® which also allows the non-gravimetric determination of the K_v, although this sensor was not used in this study. Additionally, only a small amount of actual product is needed to obtain the R_p profile. This is recommended when dealing with very expensive materials or with

new formulations that need to be further studied, saving time for batch preparation.

This study presented only the use of these tools applied to the design space estimation for central batch conditions. Additionally, the study considered only a static environment and did not include uncertainties, derived from batch variability, into the design space. All these non-explored approaches may be included in future research. Additionally, future work could explore a combined alternative of a non-gravimetric K_v estimation in a very small scale in a MicroFD®. This way all advantages of the proposed novel tools would be retained while removing the limitations of each approach.

ACKNOWLEDGEMENT AND DISCLOSURES

The authors would like to acknowledge Millrock Technology, Inc., for the financial support and the useful suggestions for the use of the device. The contribution of Domenico Colucci to the IR camera setting is gratefully acknowledged by the authors.

FUNDING

Open access funding provided by Politecnico di Torino within the CRUI-CARE Agreement. Millrock Technology, Inc., has supported the study by loaning the MicroFD® unit used in this study to the research group of the Politecnico di Torino, and by helping the researchers to solve practical issues related to the experimental investigation.

REFERENCES

1. Fissore D. Freeze Drying of Pharmaceuticals. Encycl Pharm Sci Technol. 4th ed. New York, NY: Taylor and Francis; 2013. p. 1723–37.
2. Velardi SA, Rasetto V, Barresi AA. Dynamic parameters estimation method: advanced manometric temperature measurement approach for freeze-drying monitoring of pharmaceutical solutions. Ind Eng Chem Res. 2008;47:8445–57.
3. Meg LaTorre-Snyder. Lyophilization: The Basics. An overview of the lyophilization process as well as the advantages and disadvantages. Pharm Process. 2017;32.
4. Patel SM, Doen T, Pikal MJ. Determination of end point of primary drying in freeze-drying process control. AAPS PharmSciTech. 2010;11:73–84.
5. Beirowski J, Inghelbrecht S, Arien A, Gieseler H. Freeze drying of Nanosuspensions, 2: the role of the critical formulation temperature on stability of drug Nanosuspensions and its practical implication on process design. J Pharm Sci. 2011;100:4471–81.
6. Colandene JD, Maldonado LM, Creagh AT, Vrettos JS, Goad KG, Spitznagel TM. Lyophilization cycle development for a high-concentration monoclonal antibody formulation lacking a crystalline bulking agent. J Pharm Sci. 2007;96:1598–608.
7. Horn J, Friess W. Detection of collapse and crystallization of saccharide, protein, and mannitol formulations by optical fibers in lyophilization. Front Chem. 2018;6:1–9.
8. Stratta L, Capozzi LC, Franzino S, Pisano R. Economic analysis of a freeze-drying cycle. Processes. 2020;8:1–17.
9. Haeuser C, Goldbach P, Huwyler J, Friess W, Allmendinger A. Be aggressive! Amorphous excipients enabling single-step freeze-drying of monoclonal antibody formulations. Pharmaceutics. 2019;11:1–16.
10. Patel SM, Pikal MJ. Lyophilization process design space. J Pharm Sci. 2013;102:3883–7.
11. Nail SL, Searles JA. Elements of quality by design in development and scale-up of freeze-dried parenterals. BioPharm Int. 2008;21:44–52.
12. Patel SM, Chaudhuri S, Pikal MJ. Choked flow and importance of Mach I in freeze-drying process design. Chem Eng Sci. Elsevier. 2010;65:5716–27.
13. Fissore D, Barresi AA. Scale-up and process transfer of freeze-drying recipes. Dry Technol. 2011;29:1673–84.
14. Bourlés E, Lannoy G, de Scutellà B, Fonseca F, Trelea IC, Passot S. Lyophilization of Pharmaceuticals and Biologicals. Methods in Pharmacology and Toxicology. In: K. W, P. M, editors. New York, NY: Humana Press; 2019. p. 215–40.
15. Pikal MJ, Roy ML, Shah S. Mass and heat transfer in vial freeze-drying of pharmaceuticals: role of the vial. J Pharm Sci. 1984;73:1224–37.
16. Scutellà B, Passot S, Bourlés E, Fonseca F, Tréléa IC. How vial geometry variability influences heat transfer and product temperature during freeze-drying. J Pharm Sci. 2017;106:770–8.
17. Scutellà B, Bourlès E. Development of freeze-drying cycle via design space approach: a case study on vaccines. J Pharm Sci. Elsevier ltd; 2020;25(10):1302–13.
18. Fissore D, Pisano R, Barresi AA. Using mathematical modeling and prior knowledge for QbD in freeze-drying processes. Jameel F, editor. Qual. By des. Biopharm. Drug prod. Dev. New York: Springer Science; 2015.
19. Pisano R, Fissore D, Barresi AA. Heat Transfer in Freeze-Drying Apparatus. In: Dr. Bernardes MADS, editor. Dev Heat Transf. 1st ed.: InTech; 2011. p. 91–114.
20. Hibler S, Wagner C, Gieseler H. Vial freeze-drying, part 1: new insights into heat transfer characteristics of tubing and molded vials. J Pharm Sci. 2012;101:1189–201.
21. Chouvenc P, Vessot S, Andrieu J, Vacus P. Optimization of the freeze-drying cycle: a new model for pressure rise analysis. Dry Technol. 2004;22:1577–601.
22. Tang XC, Nail SL, Pikal MJ. Evaluation of manometric temperature measurement (MTM), a process analytical technology tool in freeze drying, part III: heat and mass transfer measurement. AAPS PharmSciTech. 2006;7.

23. Fissore D, Pisano R, Barresi AA. On the methods based on the pressure rise test for monitoring a freeze-drying process. Dry Technol. 2011;29:73–90.
24. Carfagna M, Rosa M, Lucke M, Hawe A, Frieß W. Heat flux sensor to create a design space for freeze-drying development. Eur J pharm Biopharm. Elsevier; 2020;153:84–94.
25. Gieseler H, Kessler WJ, Finson M, Davis SJ, Mulhall PA, Bons V, et al. Evaluation of tunable diode laser absorption spectroscopy for in-process water vapor mass flux measurements during freeze drying. J Pharm Sci. 2007;96:1776–93.
26. Kuu WY, Nail SL, Sacha G. Rapid determination of vial heat transfer parameters using tunable diode laser absorption spectroscopy (TDLAS) in response to step-changes in pressure set-point during freeze-drying. J Pharm Sci. 2009;98:1136–53.
27. Korpus C, Pikal M, Friess W. Heat transfer analysis of an optimized, flexible holder system for freeze-drying in dual chamber cartridges using different state-of-the-art PAT tools. J pharm Sci. Elsevier ltd; 2016;105:3304–13.
28. Scutellà B, Trelea IC, Bourlés E, Fonseca F, Passot S. Determination of the dried product resistance variability and its influence on the product temperature in pharmaceutical freeze-drying. Eur J pharm Biopharm. Elsevier ltd; 2018;128:379–88.
29. Kuu WY, Obryan KR, Hardwick LM, Paul TW. Product mass transfer resistance directly determined during freeze-drying cycle runs using tunable diode laser absorption spectroscopy (TDLAS) and pore diffusion model. Pharm Dev Technol. 2011;16:343–57.
30. Goldman JM, Chen X, Register JT, Nesarikar V, Iyer L, Wu Y, et al. Representative scale-down lyophilization cycle development using a seven vial freeze-dryer MicroFD. J Pharm Sci. 2019;108:1486–95.
31. Pisano R. Automatic control of a freeze-drying process: detection of the end point of primary drying. Dry Technol. Taylor & Francis; 2020;1–18.
32. Fissore D, Pisano R, Barresi AA. Process analytical technology for monitoring pharmaceuticals freeze-drying – a comprehensive review. Dry Technol. 2018;36:1–27.
33. Harguindeguy M, Fissore D. Temperature/end point monitoring and modelling of a batch freeze-drying process using an infrared camera. Eur J Pharm Biopharm. 2020.
34. Velardi SA, Barresi AA. Development of simplified models for the freeze-drying process and investigation of the optimal operating conditions. Chem Eng Res Des. 2008;86:9–22.
35. Fissore D, Harguindeguy M, Ramirez DV, Thompson TN. Development of freeze-drying cycles for pharmaceutical products using a micro freeze-dryer. J pharm Sci. Elsevier ltd; 2019;109:797–806.
36. Fissore D, Pisano R, Barresi AA. Advanced approach to build the design space for the primary drying of a pharmaceutical freeze-drying process. J Pharm Sci. 2011;100:4923–33.
37. Fissore D, Pisano R. Computer-aided framework for the design of freeze-drying cycles: optimization of the operating conditions of the primary drying stage. Processes. 2015;3:406–21.
38. Giordano A, Barresi AA, Fissore D. On the use of mathematical models to build the design space for the primary drying phase of a pharmaceutical lyophilization process. J pharm Sci. Elsevier Masson SAS; 2011;100:311–24.
39. Bosca S, Fissore D. Design and validation of an innovative soft-sensor for pharmaceuticals freeze-drying monitoring. Chem Eng Sci. 2011;66:5127–36.
40. Lide DR. Properties of ice and supercooled water. In: Haynes WM, editor. CRC Handb Chem Phys. 90th Editi. Boca Raton, FL: CRC press, Taylor & Francis Group; 2010. p. 6–12.
41. Tang X, Nail SL, Pikal MJ. Freeze-drying process design by manometric temperature measurement: design of a smart freeze-dryer. Pharm Res. 2005;22:685–700.
42. Sundaram J, Shay YHM, Hsu CC, Sane SU. Design space development for lyophilization using doe and process modeling. BioPharm Int. 2010;23:40–5.
43. Demichela M, Barresi AA, Baldissone G. The effect of human error on the temperature monitoring and control of freeze drying processes by means of thermocouples. Front Chem. 2018;6:1–11.
44. Gan KH, Bruttini R, Crosser OK, Liapis AI. Heating policies during the primary and secondary drying stages of the lyophilization process in vials: effects of the arrangement of vials in clusters of square and hexagonal arrays on trays. Dry Technol. 2004;22:1539–75.
45. Aydin D, Memmedli M, Omay RE. Smoothing parameter selection for nonparametric regression using smoothing spline. Eur J Pure Appl Math. 2013;6:222–38.
46. Fissore D, Gallo G, Ruggiero AE, Thompson TN. On the use of a micro freeze-dryer for the investigation of the primary drying stage of a freeze-drying process. Eur J pharm Biopharm. Elsevier; 2019;141:121–9.
47. Horn J, Friess W. Detection of collapse and crystallization of saccharide, Protein , and Mannitol Formulations by Optical Fibers in Lyophilization. 2018;6:1–9.
48. Kim AI, Akers MJ, Nail SL. The physical state of mannitol after freeze-drying: effects of mannitol concentration, freezing rate, and a noncrystallizing cosolute. J Pharm Sci. 1998;87:931–5.
49. Barresi A, Ghio S, Fissore D, Pisano R. Freeze drying of pharmaceutical excipients close to collapse temperature: influence of the process conditions on process time and product quality. Dry Technol. 2009;27:805–16.
50. Cavatur RK, Vemuri NM, Pyne A, Chrzan Z, Toledo-Velasquez D, Suryanarayanan R. Crystallization behavior of mannitol in frozen aqueous solutions. Pharm Res. 2002;19:894–900.
51. Pyne A, Surana R, Suryanarayanan R. Crystallization of mannitol below Tg′ during freeze-drying in binary and ternary aqueous systems. Pharm Res. 2002;19:901–8.
52. Maity A, Sherman M. The two-sample t test with one variance unknown. Am Stat. 2006;60:163–6.
53. Tang X, Pikal MJ. Design of Freeze-Drying Processes for pharmaceuticals: practical advice. Pharm Res. 2004;21:191–200.